A Sensitization-Free Dimethyl Fumarate Prodrug, Isosorbide Di-(Methyl Fumarate), Provides a Topical Treatment Candidate for Psoriasis

Krzysztof Bojanowski[1,2], Collins U. Ibeji[3], Parvesh Singh[4], William R. Swindell[5] and Ratan K. Chaudhuri[2,6]

Dimethyl fumarate (DMF) is an effective oral treatment for psoriasis administered in Europe for nearly 60 years. However, its potential has been limited by contact dermatitis that prohibits topical application. This paper characterizes a DMF derivative, isosorbide DMF (IDMF), which was designed to have antipsoriatic effects without skin-sensitizing properties. We show that IDMF exhibits neither genotoxicity nor radiation sensitivity in skin fibroblasts and is nonirritating and nonsensitizing in animal models (rat, rabbit, guinea pig). Microarray analysis of cytokine-stimulated keratinocytes showed that IDMF represses the expression of genes specifically upregulated in psoriatic skin lesions but not those of other skin diseases. IDMF also downregulated genes induced by IL-17A and TNF in keratinocytes as well as predicted targets of NF-κB and the antidifferentiation noncoding RNA (i.e., *ANCR*). IDMF further stimulated the transcription of oxidative stress response genes (*NQO1*, *GPX2*, *GSR*) with stronger NRF2/ARE activation compared to DMF. Finally, IDMF reduced erythema and scaling while repressing the expression of immune response genes in psoriasiform lesions elicited by topical application of imiquimod in mice. These data show that IDMF exhibits antipsoriatic activity that is similar or improved compared with that exhibited by DMF, without the harsh skin-sensitizing effects that have prevented topical delivery of the parent molecule.

JID Innovations (2021);**1:**100040 doi:10.1016/j.xjidi.2021.100040

INTRODUCTION

Psoriasis vulgaris is a chronic immune-mediated disease causing harmful deregulation of the epidermis leading to plaque formation (Lowes et al., 2014). There has been tremendous progress in the treatment of moderate-to-severe psoriasis in recent decades, most significantly related to the advancement of systemic biologic therapies (Kim and Lebwohl, 2019). Despite this progress, substantial challenges remain (Kragballe et al., 2014). Systemic biologic therapies are expensive and require close clinical monitoring, and the same biologic may lose effectiveness over time or may only partially control disease activity (Veilleux and Shear, 2017). Most notably, the use of biologic therapy for mild psoriasis is not recommended (Kim et al., 2017). Moreover, patients with moderate-to-severe disease on biologic therapy may still require topical medications, which may be needed to limit the dose of the biologic required (Bagel and Gold, 2017). Topical therapies for psoriasis such as corticosteroids, emollients, vitamin D analogs, coal tar, and retinoids are frequently prescribed (Menter et al., 2009). However, these treatments have been available for decades, and development of new topical treatments has lagged relative to that of systemic agents.

Fumaric acid ester derivatives, such as monoethyl fumarate and dimethyl fumarate (DMF), have been approved in Europe for psoriasis treatment since 1994 (Altmeyer et al., 1994). More recently, a DMF-only oral formulation (Skilarence) was approved by the European Medicines Agency as a systemic psoriasis treatment (Mrowietz et al., 2017). Although a topical fumaric acid ester therapy had been developed in earlier decades (Schäfer, 1984), the use of topical fumaric acid derivatives has not been successful in the treatment of psoriasis, primarily because these compounds have harsh cutaneous effects. For example, both monoethyl fumarate and DMF were reported to cause itching with maculopapular erythema around psoriasis lesions (Nieboer et al., 1989), with

[1]*Sunny BioDiscovery, Inc, Santa Paula, California, USA;* [2]*Symbionyx Pharmaceuticals Inc, Boonton, New Jersey, USA;* [3]*Department of Pure and Industrial Chemistry, Faculty of Physical Sciences, University of Nigeria, Nsukka, Nigeria;* [4]*School of Chemistry & Physics, University of KwaZulu-Natal, Durban, South Africa;* [5]*Department of Internal Medicine, The Jewish Hospital, Cincinnati, Ohio, USA; and* [6]*Sytheon Ltd, Boonton, New Jersey, USA*

Correspondence: William R. Swindell, Department of Internal Medicine, The Jewish Hospital, 4777 East Galbraith Road, Cincinnati, Ohio 45236-2725, USA. E-mail: ws277814@ohio.edu

Abbreviations: ARE, antioxidant response element; CES2, carboxylesterase 2; CPD, cyclobutane pyrimidine dimer; CTRL, control; DEG, differentially expressed gene; DMF, dimethyl fumarate; FC, fold change; FDR, false discovery rate; GSH, glutathione; IDMF, isosorbide di-(methyl fumarate); IMQ, imiquimod; KC, keratinocyte; MMF, monomethyl fumarate; PN, uninvolved skin from psoriasis patient; PP, lesional skin from psoriasis patient; RNA-seq, RNA sequencing; VEH, vehicle

Received 12 April 2021; revised 28 May 2021; accepted 7 June 2021; accepted manuscript published online XXX; corrected proof published online XXX

Cite this article as: JID Innovations 2021;1:100040

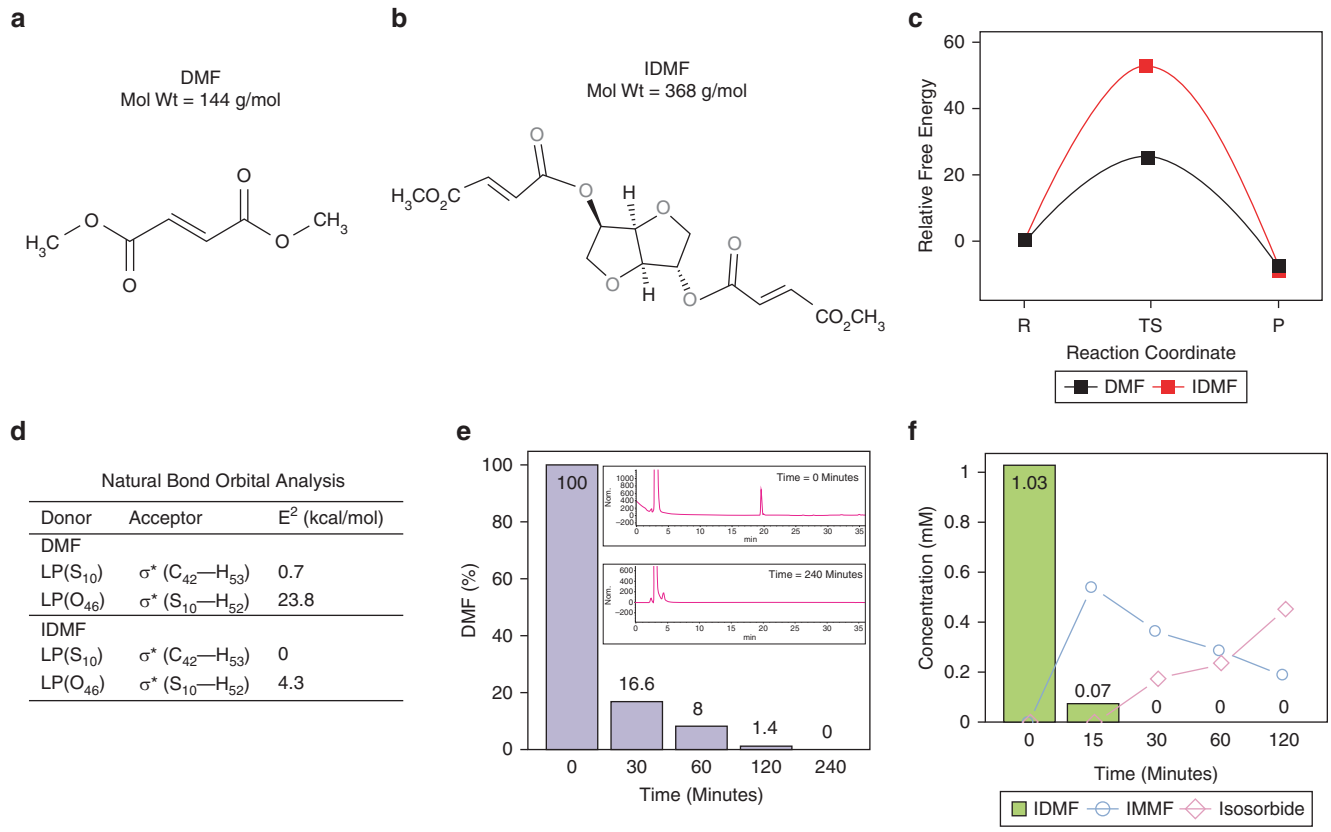

Donor	Acceptor	E^2 (kcal/mol)
DMF		
$LP(S_{10})$	σ^* (C_{42}—H_{53})	0.7
$LP(O_{46})$	σ^* (S_{10}—H_{52})	23.8
IDMF		
$LP(S_{10})$	σ^* (C_{42}—H_{53})	0
$LP(O_{46})$	σ^* (S_{10}—H_{52})	4.3

Figure 1. IDMF stability and cutaneous metabolism. (**a**) DMF structure. (**b**) IDMF structure. (**c**) Gibbs free energy pathway of S—H group attack of C=C of DMF and IDMF obtained at B3LYP /6-31+G(d,p). (**d**) Natural bond orbital analysis. Stabilization energies of the second-order perturbation theory corresponding to the main intermolecular charge transfer interaction (donor to acceptor) of S—H group attack of C=C on the DMF and IDMF transition state at B3LYP /6-31+G(d,p). (**e**) DMF fatty acid ester hydrolysis during incubation with CES2 enzyme. The percentage of DMF remaining is shown at different time points (chromatograms, upper right) (**f**) IDMF fatty acid ester hydrolysis during incubation with CES2 enzyme. The concentration of IDMF is shown along with that of its metabolites (IMMF and isosorbide). CES2, carboxylesterase 2; DMF, dimethyl fumarate; IDMF, isosorbide di-(methyl fumarate); IMMF, isosorbide monomethyl fumarate; LP, lone pair; Mol Wt, molecular weight; P, product; R, reactant; TS, transition state.

similar reactions seen in normal human and animal skin (Gehring and Gloor, 1990; Lahti and Maibach, 1985). Despite this, in vitro studies using keratinocytes (KCs) have shown that DMF and/or monomethyl fumarate (MMF) have antiproliferative and prodifferentiation effects at subtoxic concentrations (Helwa et al., 2015; Sebök et al., 1994). Such work has also shown anti-inflammatory effects of DMF and MMF (Helwa et al., 2015; Stoof et al., 2001). The principle of topical fumaric acid ester derivative therapy for psoriasis thus remains plausible despite the obstacle of skin irritation.

We have synthesized isosorbide DMF (IDMF), a prodrug of DMF, with the goal of preserving antipsoriatic activity while eliminating skin sensitization side effects of the parent molecule (Chaudhuri and Bojanowski, 2017). IDMF was designed using a structure–activity modeling approach (Becke, 1993; Kohn et al., 1996). This strategy allowed us to identify a fumarate with higher activation energy, which could be administered both orally and topically, with significantly less skin irritation potential owing to decreased reactivity. A recent study performed using cultured astrocytes showed that IDMF-repressed transcription of genes mediating mitosis and proliferation and further suppressed the gene expression patterns associated with inflammation and oxidative stress (Swindell et al., 2020). However, the effects of IDMF on a psoriasis-relevant cutaneous cell type (e.g., KCs) have not yet been reported in a peer-reviewed study, and likewise, research supporting the safety and tolerability of IDMF as a topical agent has not been published.

This work presents studies evaluating the cutaneous effects of IDMF using both in vitro and in vivo models. Our findings provide preclinical data to support the safety of topical application and show that IDMF lacks harsh cutaneous effects. We characterize molecular-level mechanisms of IDMF in psoriasis-relevant cells to show that IDMF possesses antipsoriatic activity. These findings provide proof of concept to support IDMF as a candidate for further development as a topical psoriasis vulgaris treatment.

RESULTS

IDMF stability and cutaneous metabolism

We investigated the interaction of DMF (Figure 1a) and IDMF (Figure 1b) with glutathione (GSH) using quantum mechanics calculations and the density functional theory method (Becke, 1993; Kohn et al., 1996). The ground state molecular structure of GSH and the alkene group (C=C) of DMF and IDMF was subjected to density functional theory to evaluate the bond-forming and -breaking mechanisms. IDMF was predicted to be considerably less reactive than DMF owing to

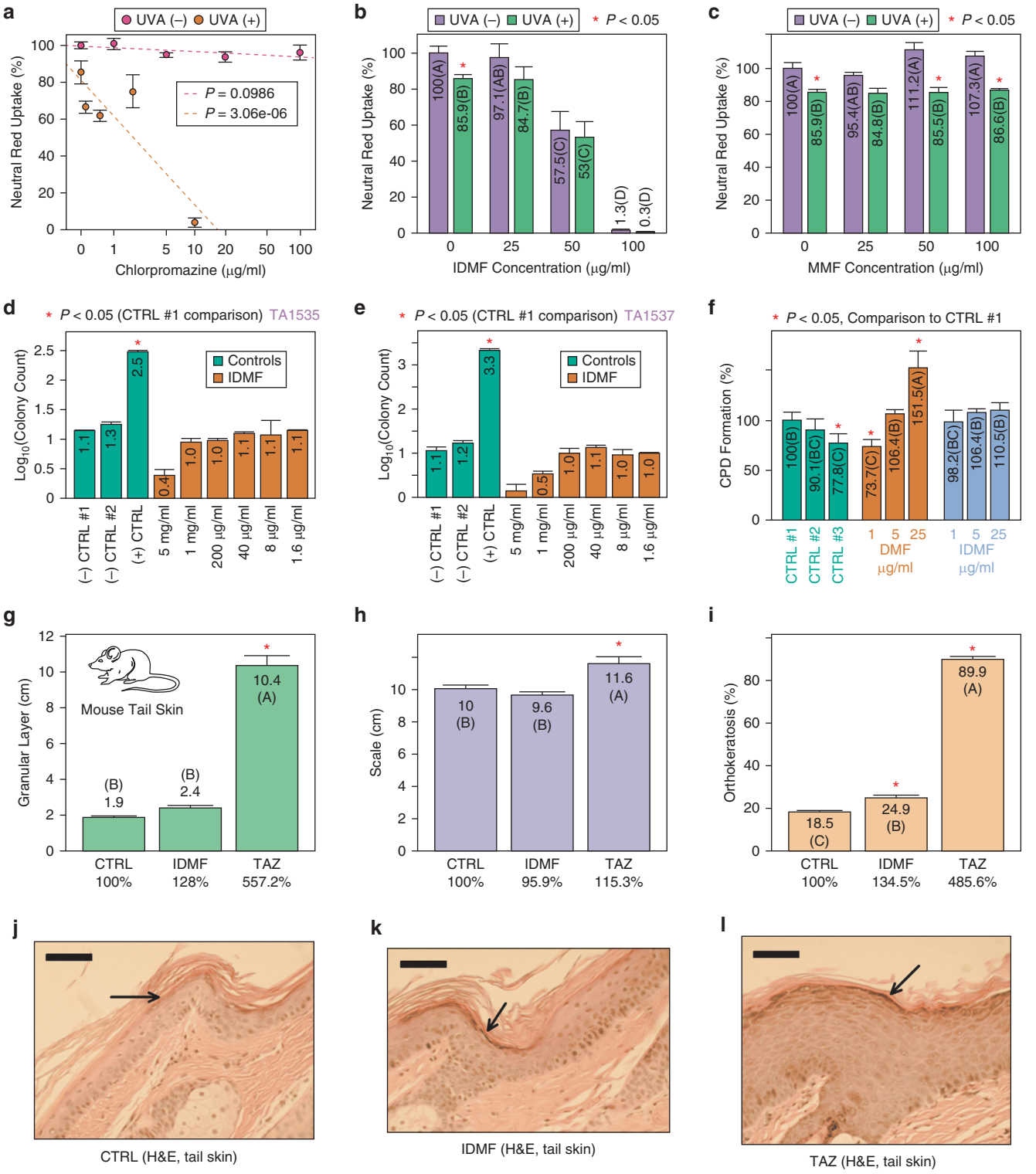

Figure 2. IDMF skin toxicity. (**a–c**) Phototoxicity (n ≥ 4 per treatment; *$P < 0.05$, UVA[–] vs. UVA[+]). (**d, e**) *Salmonella* mutagenicity ([–] CTRL #1 = water; [–] CTRL #2 = DMSO; [+] CTRL = sodium azide for **d** or acridine for **e**; n = 2 per treatment; *$P < 0.05$, [–] CTRL #1 comparison). (**f**) CPD formation (n = 3–7 per treatment; *$P < 0.05$, CTRL #1 comparison). CTRL treatments: #1 = irradiated water treated, #2 = irradiated DMF/IDMF treated, #3 = nonirradiated water treated. (**g–i**) Mouse tail skin properties (n = 3 per group; *$P < 0.05$, CTRL comparison). (**j–l**) Tail skin H&E (Bar = 100 μm; arrows indicate stratum granulosum). Treatments having the same letter in bar plots do not differ significantly ($P > 0.05$, Fisher's LSD; error bars: ±1 SE). CPD, cyclobutane pyrimidine primer; CTRL, control; DMF, dimethyl fumarate; IDMF, isosorbide di-(methyl fumarate); LSD, least significant difference; SE, standard error; TAZ, tazarotene.

its 25 kcal/mol higher activation free energy barrier (Figure 1c). This prediction was further supported by natural bond orbital analysis (Lee et al., 2013), which showed that the stabilization energy (E^2 value) of the GSH–DMF complex was >5 times greater than that of the GSH–IDMF complex (Figure 1d).

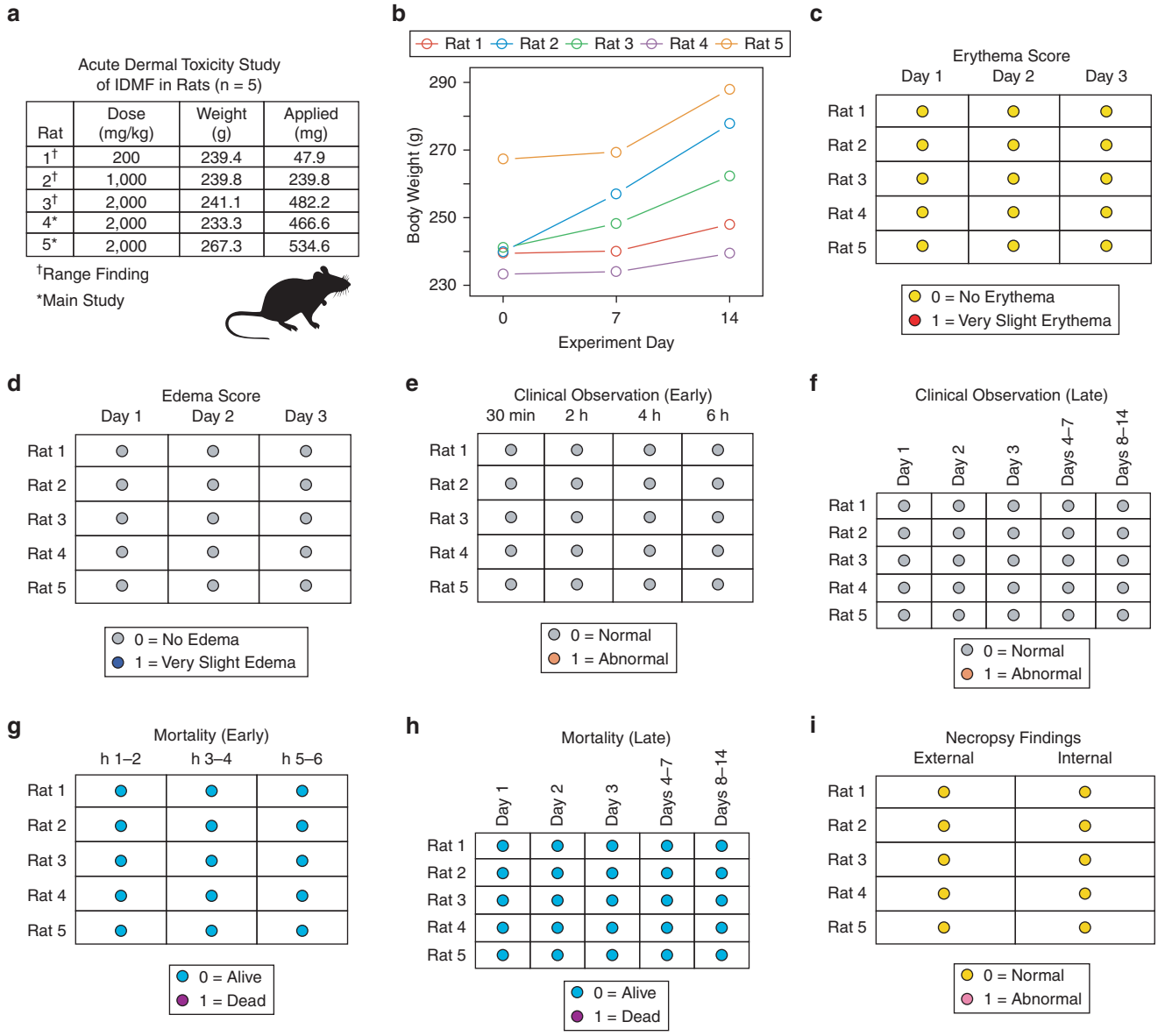

Figure 3. IDMF acute dermal toxicity study in rats. (**a**) Experimental design. (**b**) Body weights. (**c**) Erythema score. (**d**) Edema score. (**e**) Clinical observations (early, <6 h). (**f**) Clinical observations (late, 1–14 days). (**g**) Mortality (early, <6 h). (**h**) Mortality (late, 1–14 days). (**i**) Necropsy findings (external and internal). h, hour; IDMF, isosorbide di-(methyl fumarate); min, minute.

Carboxylesterase 2 (CES2) is the major carboxylesterase enzyme expressed by KCs and plays a major role in cutaneous metabolism (Zhu et al., 2007). We used chromatography to evaluate the concentration of DMF during incubation with CES2, which showed that DMF hydrolysis was >90% complete after 60 minutes of incubation (Figure 1e). IDMF also underwent significant hydrolysis during this time but was largely converted to isosorbide MMF and isosorbide derivatives. Isosorbide MMF then underwent slower hydrolysis, such that 50% of the isosorbide MMF product remained intact after 60 minutes (Figure 1f).

IDMF does not exhibit phototoxicity or genotoxicity and lacks adverse effects on mouse tail skin

Neutral red uptake assays were carried out to evaluate IDMF and MMF cytotoxicity in neonatal human dermal fibroblasts ($n \geq 4$ per treatment). The positive control chlorpromazine potently decreased the viability of UVA-treated fibroblasts ($P = 3.06e\text{-}06$) (Figure 2a). UVA treatment significantly inhibited the growth of MMF-treated cells, although this effect was not influenced by MMF treatment (Figure 2c). Likewise, IDMF treatment decreased cell viability at higher doses, although this effect was similar in UVA(–) and UVA(+) cells, consistent with a lack of phototoxicity (Figure 2b). IDMF also did not show mutagenic effects in Ames assays performed with two *Salmonella* test strains (TA1535 and TA1537), as evidenced by low levels of colony formation after exposure to varying IDMF concentrations (Figure 2d and e, $n = 2$ per treatment).

We next investigated the skin sensitization potential of IDMF by comparing its effect with that of DMF on DNA damage repair (Figure 2f). Human dermal fibroblasts were

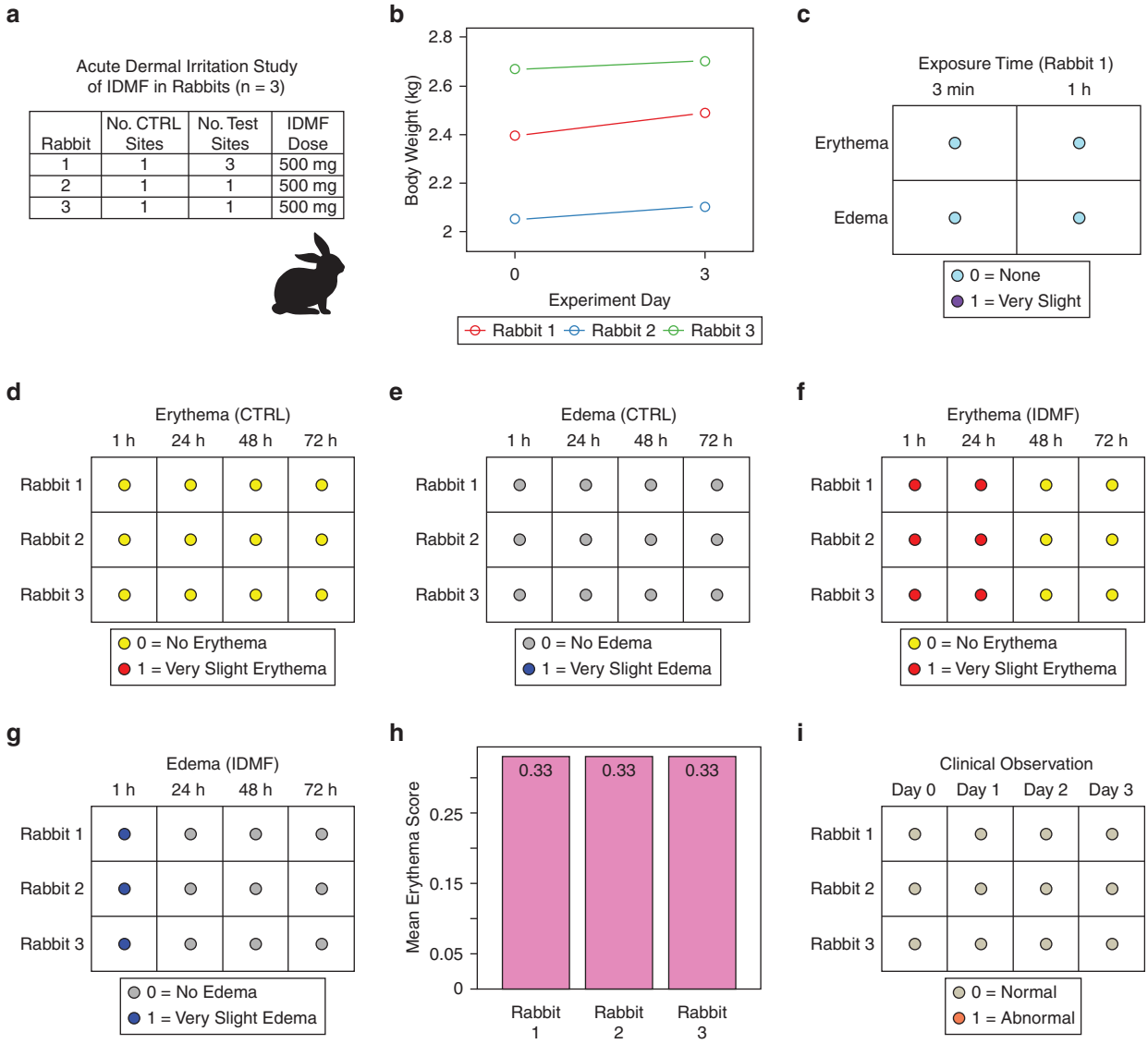

Figure 4. IDMF acute dermal irritation study in rabbits. (**a**) Experimental design. (**b**) Body weight. (**c**) Erythema and edema 3-min and 1-h exposure sites (rabbit 1). (**d–g**) Erythema and edema at CTRL- or IDMF-treated sites (4-h exposure). (**h**) Average erythema scores (24–48 h, 4-h exposure sites). (**i**) Clinical observations after exposure. CTRL, control; h, hour; IDMF, isosorbide di-(methyl fumarate); No., number.

UVB irradiated to induce cyclobutane pyrimidine dimer (CPD) formation (n = 3–7 per treatment). A DMF concentration of 25 mcg/ml significantly impaired the repair process, leading to a significant increase in nonrepaired CPDs 3 hours after irradiation (Figure 2f). However, the number of nonrepaired CPDs did not differ significantly between IDMF- and water-treated cells (Figure 2f).

IDMF was then applied to mouse tail skin over a 2-week period to evaluate macroscopic and histologic effects (n = 3 per group). IDMF did not cause erythema or increase skin scale (Figure 2h), but it did increase granular layer by 28% (Figure 2g and j–l) and orthokeratosis by 34.5% (Figure 2i). Notably, we did not observe a leukocytic infiltrate, parakeratosis, or hyperkeratosis. In contrast, the positive control (0.1% tazarotene) extended stratum granulosum coverage (Figure 2l) but led to hyperkeratosis, spongiosis, and widespread inflammation.

IDMF does not elicit cutaneous irritation or sensitization reactions in multiple animal models

An acute dermal toxicity study was performed in female Wistar rats with IDMF applied at 200–2,000 mg/kg (Figure 3a and b). Rats were treated with IDMF for 24 hours and were observed for 2 weeks (n = 5). No erythema or edema was observed 1–3 days after IDMF treatment (Figure 3c and d), and no treatment-related clinical signs or mortality was observed over 2 weeks (Figure 3e and f). Necropsies performed after killing yielded no abnormalities (Figure 3i).

An acute dermal irritation study was next performed by exposing male New Zealand White rabbits to 500 mg IDMF for 3 minutes, 1 hour, and 4 hours (n = 3 total) (Figure 4a and b). No immediate reaction was observed after 3-minute or 1-hour exposures (Figure 4c). Only very slight erythema was observed after the 4-hour IDMF exposure, which was no longer evident after 48 hours (Figure 4e, f, and h). Likewise, very slight edema

a

Skin Sensitization Study of IDMF in Guinea Pigs

Group	Flank	Induction Phase	Challenge Phase
		Days 0, 7, 14	Day 28
CTRL	Right	Untreated	Treatment #3
	Left	Treatment #1	Untreated
IDMF	Right	Untreated	Treatment #3
	Left	Treatment #2	Untreated

Treatment #1: 0.2 ml 80% ethanol
Treatment #2: 100 mg IDMF + 0.2 ml 80% ethanol
Treatment #3: 100 mg IDMF + 0.2 ml acetone

b

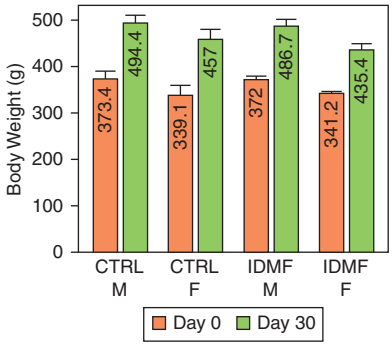

c

Number of Guinea Pigs Showing Skin Response

Group	Time (h)	Skin Response Score			
		0	1	2	3
CTRL	30	10	0	0	0
	54	10	0	0	0
IDMF	30	20	0	0	0
	54	20	0	0	0

0 = No visible change
1 = Discrete/patchy erythema
2 = Moderate/confluent erythema
3 = Intense erythema/swelling

d

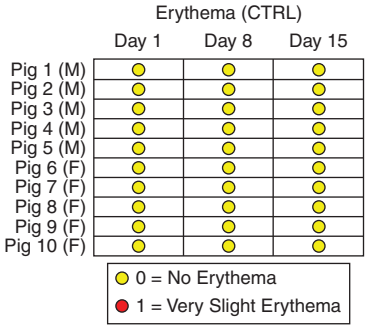

e

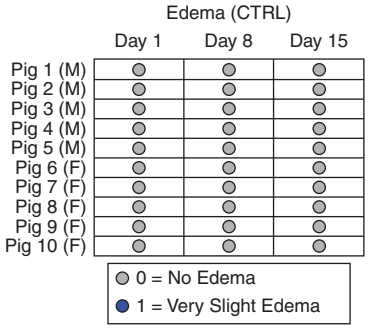

f

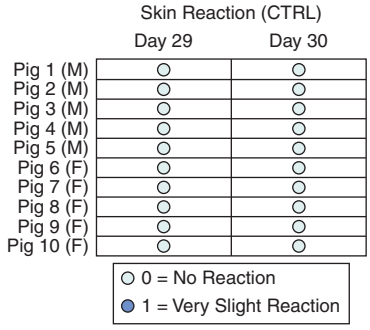

g

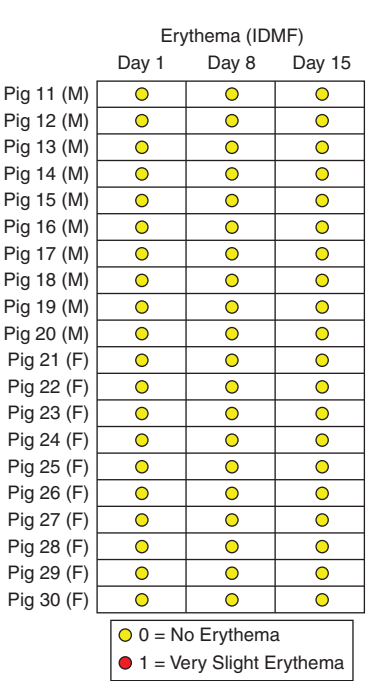

h

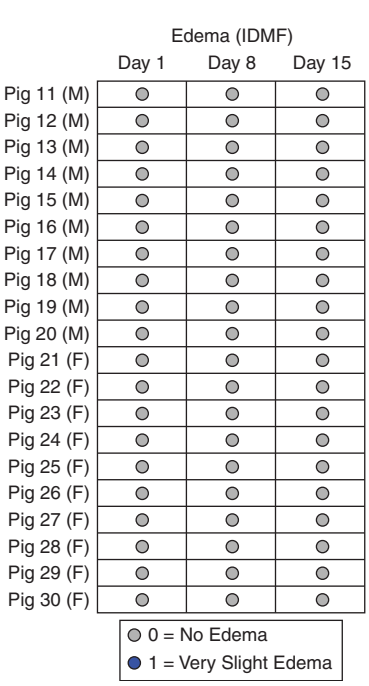

i

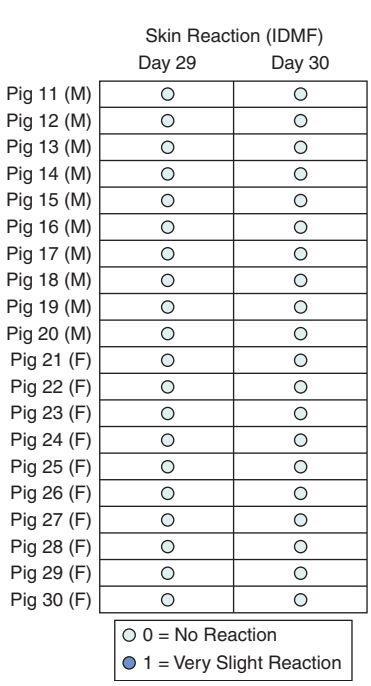

Figure 5. Skin sensitization study of IDMF in guinea pigs. (**a**) Experimental design. (**b**) Mean body weight ± 1 standard error (n = 10–30 per group). (**c**) Summary of skin reactions. The number of guinea pigs for each score is shown 30 and 54 h from the time of application after challenge exposure. (**d**) Erythema (CTRL group). (**e**) Edema (CTRL group). (**f**) Skin reaction (CTRL group). (**g**) Erythema (IDMF group). (**h**) Edema (IDMF group). (**i**) Skin reaction (IDMF group). **d**, **e**, **g**, and **h** show the skin reactions after topical application (induction) on days 1, 8, and 15 for individual guinea pigs. **f** and **i** show skin reactions after challenge application on days 29 (30 h) and 30 (54 h) for individual guinea pigs. CTRL, control; F, female; h, hour; IDMF, isosorbide di-(methyl fumarate); M, male.

was present after the 4-hour exposure but was no longer discernable after 24 hours (Figure 4e and g). No abnormal clinical findings were noted for 3 days after exposure (Figure 4i).

A skin sensitization study was next performed using Hartley strain guinea pigs (n = 30 in total) (Figure 5a and b). A topical induction dose of 100 mg IDMF was applied (days 0, 7, and 14) with an additional 100 mg challenge application on day 28 (Figure 5a). No erythema or edema was observed on days 1, 8, and 15 in either group after a topical application on the previous day (Figure 5d, e, g, and h).

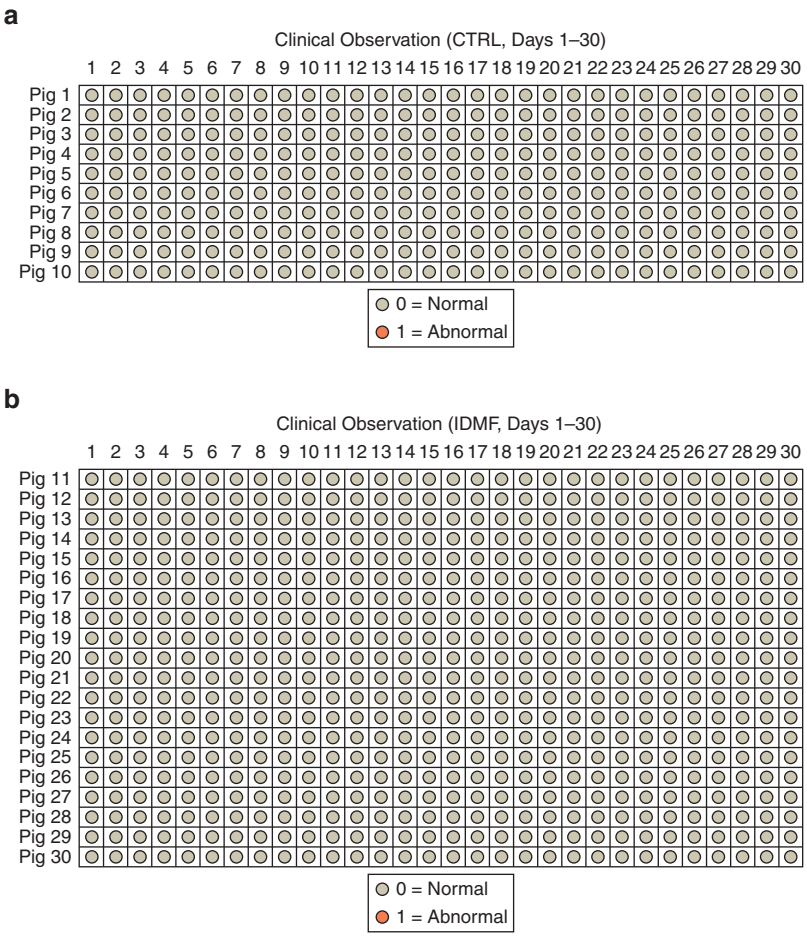

Figure 6. Clinical observations of individual guinea pigs (days 0–30). (**a**) CTRL group (n = 10). (**b**) IDMF group (n = 20). Day 0 represents the day of dosing. CTRL, control; IDMF, isosorbide di-(methyl fumarate).

Likewise, visual observation for 2 days after challenge application on day 28 did not reveal any positive response (Figure 5c, f, and i). No treatment-related clinical signs were observed over 30 days (Figure 6).

IDMF upregulates genes mediating oxidative stress response and represses transcription of the genes associated with immune response and epithelial differentiation

DNA microarrays were used to evaluate gene expression changes in cytokine-stimulated KCs (IL-17A + IL-22 + TNF) treated with IDMF or water control for 24 hours (n = 2 per treatment). We identified 196 differentially expressed genes (DEGs), including 140 IDMF-increased DEGs (false discovery ratio [FDR] < 0.10 with fold change [FC] > 1.50) and 56 IDMF-decreased DEGs (FDR < 0.10 with FC < 0.67). Genes most strongly upregulated by IDMF included *SPP1*; *MAP2*; *AKR1C3*; *NQO1*; *PIR;* and *TCHH* (Figure 7b, c, and e). Genes most strongly downregulated by IDMF included *SLC6A14*, *SERPINB4*, *CD200*, *ABCG1*, *LMO7*, and *MRGPRX3* (Figure 7b, d, and f). The set of 140 IDMF-increased DEGs was associated with xenobiotic metabolism, response to oxidative stress, and GSH metabolism (Figure 7g and i). The set of 56 IDMF-decreased genes was associated with immune system processes, IFN-1 response, and epithelial cell differentiation (Figure 7h and j).

IDMF represses the expression of genes specifically upregulated in lesional psoriatic skin

We hypothesized that the treatment of KCs with IDMF would downregulate the expression of genes with elevated expression in lesional skin from psoriasis patients (PP) compared to uninvolved skin from psoriasis patients (PN). This comparison was appropriate because genes having elevated expression in psoriasis lesions are predominantly expressed by KCs (Swindell et al., 2014). FCs (PP/PN) from a microarray meta-analysis of 237 patients (Swindell et al., 2015b) were negatively correlated with those from IDMF-treated KCs (r = –0.129, P = 3.87e-39) (Figure 8a). This negative association was weaker on the basis of the Spearman correlation coefficient (r_s = –0.019), although it remained marginally significant (P = 0.051) (Figure 8a). A similar negative association was obtained when the IDMF KC signature was compared with the signature from an RNA sequencing (RNA-seq)-based meta-analysis of PP lesions (n = 44 patients) (Figure 8b) (Swindell et al., 2016).

Gene set enrichment analyses showed that 530 PP-increased DEGs identified from the RNA-seq meta-analysis (FDR < 0.10 with FC > 2.0) tended to be IDMF repressed (Figure 8c). The analysis was repeated using only PP-increased genes specifically elevated in psoriasis lesions (on the basis of the Psoriasis Specificity Index), which excluded genes generically elevated in lesions from multiple other skin

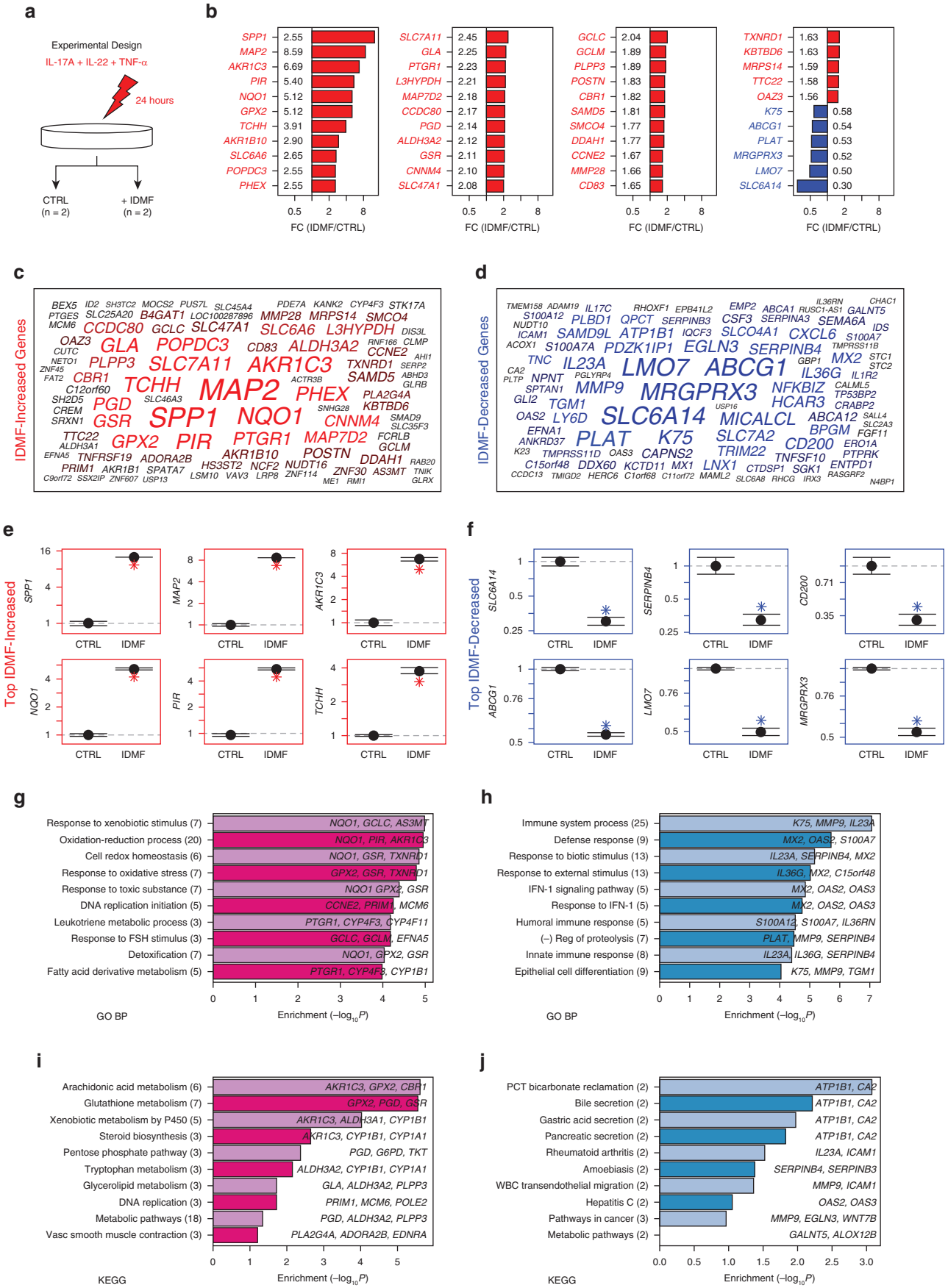

Figure 7. Differential expression summary (IDMF vs. CTRL). (**a**) Experimental design (n = 2 per group). (**b**) Top-ranked DEGs. (**c, d**) Gene clouds. Font size is inversely associated with differential expression *P*-values. (**e, f**) Average expression of top DEGs (± 1 SE; *FDR < 0.10 with FC > 1.50 or FC < 0.67). (**g, h**) GO

diseases besides psoriasis (Swindell et al., 2016). Genes specifically upregulated in psoriasis lesions were more strongly downregulated by IDMF (Figure 8c and e). There was no significant trend to indicate that the set of 310 PP-decreased genes were upregulated by IDMF in KCs (Figure 8d and f), possibly because the majority of PP-decreased genes are expressed by fibroblasts rather than by KCs (Swindell et al., 2014).

Overall, we identified 43 genes with expression inversely altered by IDMF (FDR < 0.10 with FC > 1.50 or FC < 0.67) and in PP (RNA-seq meta-analysis, FDR < 0.10 with FC > 2.0 or FC < 0.50) (Figure 8g–i). IDMF-increased/PP-decreased DEGs included *BEX5*, *ALDH3A2*, and *POSTN* (Figure 8h) and were associated with response to xenobiotic stimulus and hypoxia (Figure 8j). IDMF-decreased/PP-increased DEGs included *SLC6A14*, *SERPINB4*, and *SERPINB3* (Figure 8i) and were associated with immune/defense response, including IFN-1 signaling (Figure 8k).

IDMF reverses gene expression changes seen in KCs treated with IL-17A and TNF

IDMF-decreased/PP-increased genes encoded cytokines such as IL-23A and IL-36G (Figure 8k). We therefore asked whether the sets of cytokine-regulated genes are disproportionately increased or decreased by IDMF. The IDMF signature was compared with 59 signatures compiled from microarray studies of cytokine-treated KCs (Swindell et al., 2015a). IDMF-increased DEGs tended to be most strongly repressed by IL-17A, TNF, and IFN-γ (Figure 9a), whereas IDMF-decreased DEGs were induced by IL-17A, IFNγ, and IL-17A + TNF (Figure 9b). With respect to the IL-17A + TNF signature (GSE24767, n = 3 per treatment), the negative association was supported by a genome-wide inverse correlation of FC estimates ($r_s = -0.257$, $P = 9.77e\text{-}151$) (Figure 9c) in addition to gene set enrichment analyses (Figure 9d and e). Of the 30 genes most strongly upregulated by IDMF (i.e., lowest *P*-value), most were downregulated in KCs treated with IL-17A + TNF (Figure 9f). Of the 30 genes most strongly downregulated by IDMF (i.e., lowest *P*-value), nearly all were upregulated in KCs stimulated by IL-17A + TNF (Figure 9g). Examples of IDMF-increased/IL17A + TNF–decreased genes included *MAP2*; *NQO1*; and *KITLG* (Figure 9h), whereas examples of IDMF-decreased/IL-17A + TNF–increased genes included *SERPINB4*, *SERPINB3*, and *IL23A* (Figure 9i).

In silico promoter analysis identifies NF-κB and *ANCR* as possible mediators of IDMF-regulated gene expression

The 5 kilobase upstream regions of IDMF-regulated DEGs were evaluated to assess DNA motif enrichment (Swindell et al., 2015b). IDMF-increased DEG upstream regions were most prominently enriched for a 5′-TTTTCA/TGAATA-3′ motif interacting with IRF1 (Figure 10a), which was identified in regions upstream of IDMF-increased DEGs such as *MMP3* and *NQO1*. IDMF-decreased DEG upstream regions were most strongly enriched for a 5′-GGAAATTCCC/GGGAATTTCC-3′ motif interacting with NF-κB (Figure 10b), which was identified in regions upstream of IDMF-decreased DEGs such as *IL23A*; *MMP9*; *IL36G*; and *S100A7*. Within the *IL23A* promoter, this NF-κB motif was located 84–94 base pair upstream from the transcription start site in a conserved region (Figure 11a, e), only 7 base pair upstream from a palindromic TGANTCA element interacting with activator protein-1 (AP-1) and signal transducer and activator of transcription (STAT) that was similarly enriched in IDMF-decreased DEG upstream regions (Figure 11a–c).

Because transcription factors may cooperatively work with microRNAs and long noncoding RNAs (Dykes and Emanueli, 2017), we also identified noncoding RNA targets enriched among IDMF-regulated DEGs. MicroRNA targets most strongly enriched among IDMF-increased DEGs included hsa-miR-4733-3p and hsa-miR-433-5p (Figure 10c and d), whereas those most strongly enriched among IDMF-decreased DEGs included hsa-miR-6796-5p and hsa-miR-146a-5p (Figure 10f and g). Among long noncoding RNAs, genes annotated as *ANCR* targets were most strongly enriched with respect to both IDMF-increased and IDMF-decreased DEGs (Figure 10e and h).

IDMF activates the NRF2/antioxidant response element pathway in human embryonic kidney 293 cells

IDMF strongly upregulated the expression of oxidative stress response genes, including the NRF2 target *NQO1* (Figure 7c, e, and g). We therefore used luciferase assays to evaluate NRF2 activation in antioxidant response element (ARE)-transfected human embryonic kidney 297 cells (n = 3–6 per group). After 24 hours of IDMF treatment, we observed significant increases in the expression of the luciferase reporter gene, consistent with NRF2/ARE activation by IDMF (Figure 12). DMF also led to a significant increase in the reporter gene, but the magnitude of increase was smaller than that of IDMF at the same dose (Figure 12).

IDMF reduces skin erythema and scaling in psoriasiform mouse lesions while stimulating epidermal development pathways and repressing immune response genes

We next compared the effects of IDMF (5%) and vehicle (VEH) lotions (Table 1) on psoriasiform lesions elicited by 5% imiquimod (IMQ) cream applied to the back skin of male BALB/c mice for 5 consecutive days (n = 8 per group) (Figure 13a). IDMF was applied 1 hour after IMQ on each of the 5 days and was applied alone (without IMQ pretreatment) on day 6. As expected, 5% IMQ cream induced lesional skin formation and increased skin thickness (Figure 13b–d). IDMF significantly reduced skin erythema on days 5 and 6 ($P < 0.05$) (Figure 13b) and reduced skin scaling/flaking and skin thickness on day 6 ($P < 0.05$) (Figure 13c and d).

An exploratory RNA-seq study was performed to evaluate the effects of IDMF on IMQ-induced lesions (IMQ,

BP terms enriched among (**g**) IDMF-increased and (**h**) IDMF-decreased DEGs. **(i, j)** KEGG terms enriched among (**i**) IDMF-increased and (**j**) IDMF-decreased DEGs. In **g–j**, the number of genes associated with each term is shown in parentheses (left margin), and the exemplar genes are listed within each figure. Enrichment *P*-values (horizontal axis) were calculated using a conditional hypergeometric test. BP, biological process; CTRL, control; DEG, differentially expressed gene; FC, fold change; FDR, false discovery rate; FSH, follicular stimulating hormone; GO, Gene Ontology; IDMF, isosorbide di-(methyl fumarate); KEGG, Kyoto Encyclopedia of Genes and Genomes; PCT, proximal convoluted tubule; reg, regulation; SE, standard error; Vasc, vascular; WBC, white blood cell.

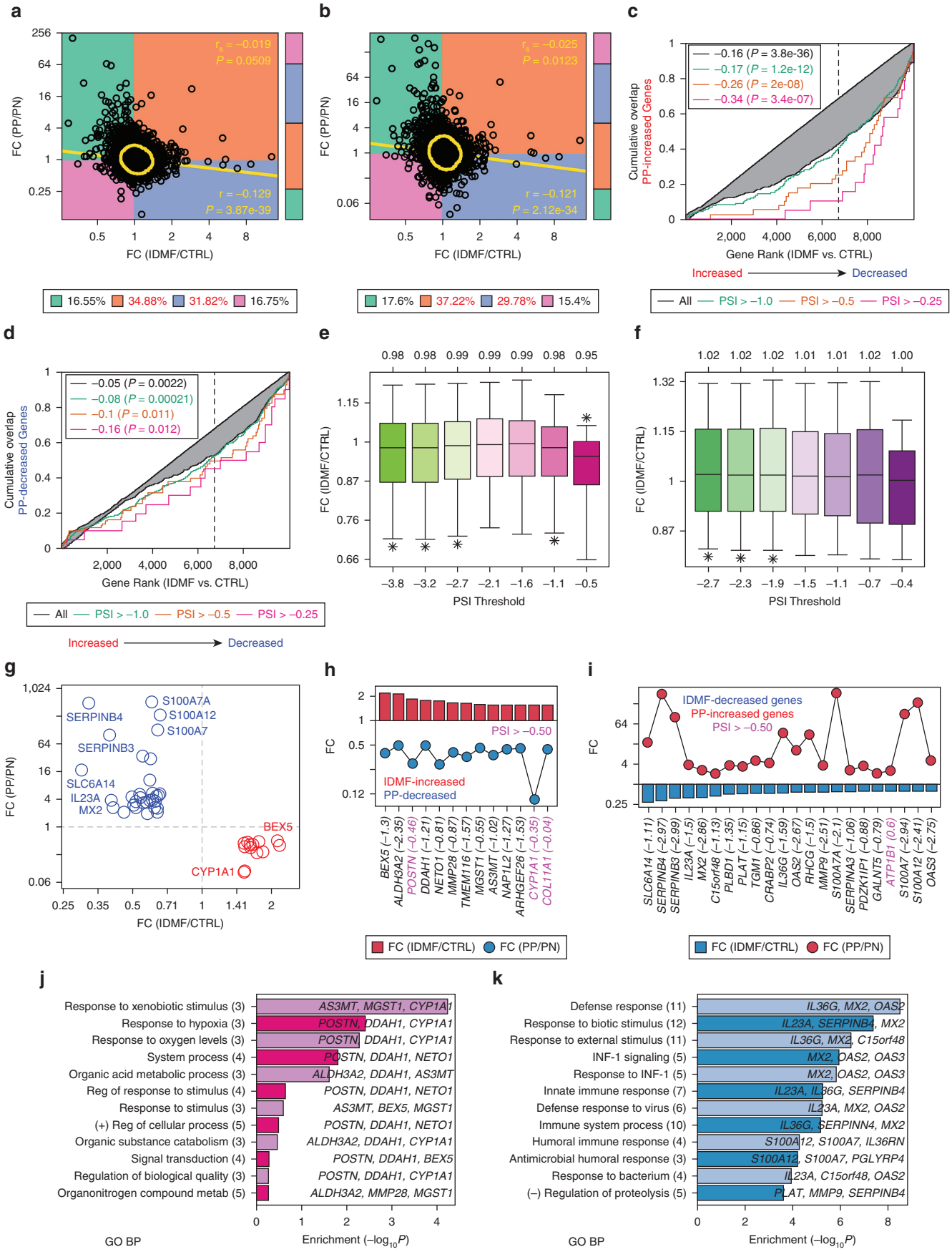

Figure 8. IDMF signature versus psoriasis transcriptome. (**a, b**) FC scatterplots (**a**: microarray, n = 237 patients; **b**: RNA-seq, n = 44 patients; top: percentage of genes/quadrant; red font: $P < 0.05$, Fisher's exact test; ellipse: middle 90% of genes, Mahalanobis distance). (**c, d**) GSEA with (**c**) PP-increased DEGs (n = 530)

n = 1; IMQ + VEH, n = 2, IMQ + IDMF, n = 1). We identified 68 genes upregulated by IDMF in IMQ-treated skin (FDR < 0.10 with FC > 1.50), along with 98 genes downregulated by IDMF (FDR < 0.10 with FC < 0.67). IDMF-increased genes included several whose orthologs had decreased expression in human psoriasis lesions, such as *Hoxd1*; *Krt36*; and *Rpl10l* (Figure 14a). Likewise, some IDMF-decreased genes had elevated expression in psoriasis lesions (e.g., *Tespa1*, *Ccr7*, *Ikzf4*) (Figure 14b). A significant fraction (73%) of genes increased by IDMF in IMQ-treated skin were downregulated in human psoriasis lesions (Figure 14c), although no trend was observed among IDMF-repressed genes (Figure 14d). As a group, the 68 genes upregulated by IDMF in IMQ-treated skin were associated with hair cycle and epidermis development (Figure 14e), whereas the 98 genes repressed by IDMF were associated with immune response activation, granulocyte migration, and immune effector process (Figure 14f).

DISCUSSION

Treatment options for psoriasis have expanded in recent decades as disease mechanisms have become better understood. However, most progress has been made in the development of systemic agents, particularly biologics, whereas less headway has been made toward the development of topical therapies. In this study, we have characterized the DMF derivative IDMF. Our preclinical findings support the use of IDMF as a candidate for topical therapy on the basis of an absence of discernable genotoxicity and phototoxicity in cultured skin cells as well as little or no sensitization in rat, rabbit, and guinea pig models. On the contrary, IDMF significantly decreased erythema and scaling in the psoriasiform lesions elicited by topical IMQ in mice, supporting both tolerability and an antipsoriatic effect. The mechanisms that mediate this effect may include repression of cytokine responses (IL-17A and TNF) and proinflammatory transcription factors (NF-κB) as well as NRF2/ARE activation. Our findings provide a rationale for early-phase clinical studies to evaluate the potential efficacy of IDMF as an antipsoriasis topical treatment.

The higher activation energy of IDMF than that of DMF (Figure 1c) likely contributes to its lower reactivity and skin sensitization potential. Because interference with DNA repair was proposed to be the principal mechanism of DMF-induced contact dermatitis (Held et al., 1991), we investigated CPD formation. CPDs constitute one of the most genotoxic lesions contributing to skin cancer and cellular senescence (Boyle et al., 2005; Mitchell, 1988; Salmon et al., 2008). As expected, DMF significantly impaired CPD repair, but in contrast, CPD formation in IDMF-treated cells did not differ significantly from that in the controls (Figure 2f). Moreover, IDMF did not induce inflammation in normal tail skin (Figure 2k), in contrast to the dermatitis-inducing retinoid tazarotene (Ma et al., 2017; Mukherjee et al., 2006). The absence of genotoxic and proinflammatory effects likely explains the lack of sensitization in animal models (rat, rabbit, guinea pig) (Figures 3–6).

Orally administered DMF is metabolized to MMF such that MMF is considered to be the active antipsoriatic metabolite, whereas DMF cannot be found circulating in the blood (Helwa et al., 2015). However, DMF has consistently been shown to have a stronger direct antiproliferative effect on KCs, which may be due in part to the unique metabolites of DMF, such as methanol (Sebök et al., 1994; Thio et al., 1994). We show a direct anti-inflammatory effect of IDMF on cytokine-stimulated KCs, with evidence for repression of key cytokine pathways such as TNF-α, IL-17A, IL-23A, IL-36G, and IFN-γ (Figures 7h, 8k, and 9a and b). These anti-cytokine effects resemble those previously described for DMF and/or MMF. For example, direct application of MMF to 12-*O*-tetradecanoylphorbol-13-acetate (TPA)–activated mouse KCs repressed the expression of *Tnfα*, *Il6*, and *Il1α* mRNAs, and in human KCs, MMF repressed TNF-α protein below the limits of detection (Helwa et al., 2015). In contrast, treatment of IFN-γ– or phorbol 12-myristate 13-acetate (PMA)–stimulated KCs with DMF repressed mRNA and protein abundance of CXCL8, CXCL9, and CXCL10 (Stoof et al., 2001). Direct anti-inflammatory effects of IDMF may thus represent a mechanism by which topical application can disrupt local inflammatory circuits to hinder the recruitment of immune cells into psoriatic lesions (Lowes et al., 2014).

It has been proposed that NF-κB inhibition serves as an NRF2-independent mechanism by which orally administered DMF improves psoriatic disease (Brück et al., 2018). Inhibition of NF-κB activity by DMF has been shown in a variety of cell types, including T cells (Gerdes et al., 2007), dermal fibroblasts (Vandermeeren et al., 2001), and KCs (Gesser et al., 2011, 2007). However, DMF is a stronger inhibitor of NF-κB than its metabolites MMF and monoethyl fumarate such that any direct action of DMF on NF-κB function in KCs would not occur when DMF is given orally (Gillard et al., 2015). Previous work has additionally shown that DMF can inhibit AP-1 in some cell types such as lung fibroblasts (Seidel et al., 2010). In our study, regions upstream of genes downregulated by IDMF were enriched for DNA motifs recognized by NF-κB and AP-1 (Figure 10b). The NF-κB motif was identified within a conserved region near the transcription start site of *IL23A* (Figure 11e), which was among the mRNAs downregulated by IDMF (Figure 7h). Therefore, similar to DMF, IDMF may repress NF-κB activity, although for IDMF, this can be achieved by topical application, leading to a reduced local expression of *IL23A* among other NF-κB targets. Potentially, these effects of IDMF may occur in coordination with other transcription factors, such as AP-1, STAT, or IRF1, which were also identified by our DNA motif analysis (Figure 10a and b).

and (**d**) PP-decreased DEGs (n = 310) (filtering by PSI threshold, RNA-seq meta-analysis). (**e, f**) FC estimates for (**e**) PP-increased and (**f**) PP-decreased DEGs (boxes: 25–75th percentiles; whiskers: 10–90th percentiles; $*P < 0.05$, comparison with 1.00, Wilcoxon test). (**g**) FC scatterplot (genes inversely altered in PP lesions vs. IDMF). (**h**) IDMF-increased/PP-decreased DEGs. (**i**) IDMF-decreased/PP-increased DEGs. (**j, k**) GO BP terms enriched among (**j**) IDMF-increased/PP-decreased and (**k**) IDMF-decreased/PP-increased DEGs (parentheses: number of genes associated with each term; exemplar genes within figures). BP, biological process; CTRL, control; DEG, differentially expressed gene; FC, fold change; GO, Gene Ontology; GSEA, Gene Set Enrichment Analysis; IDMF, isosorbide di-(methyl fumarate); metab, metabolism; PN, uninvolved skin from psoriasis patient; PP, lesional skin from psoriasis patient; PSI, Psoriasis Specificity Index; reg, regulation; RNA-seq, RNA sequencing.

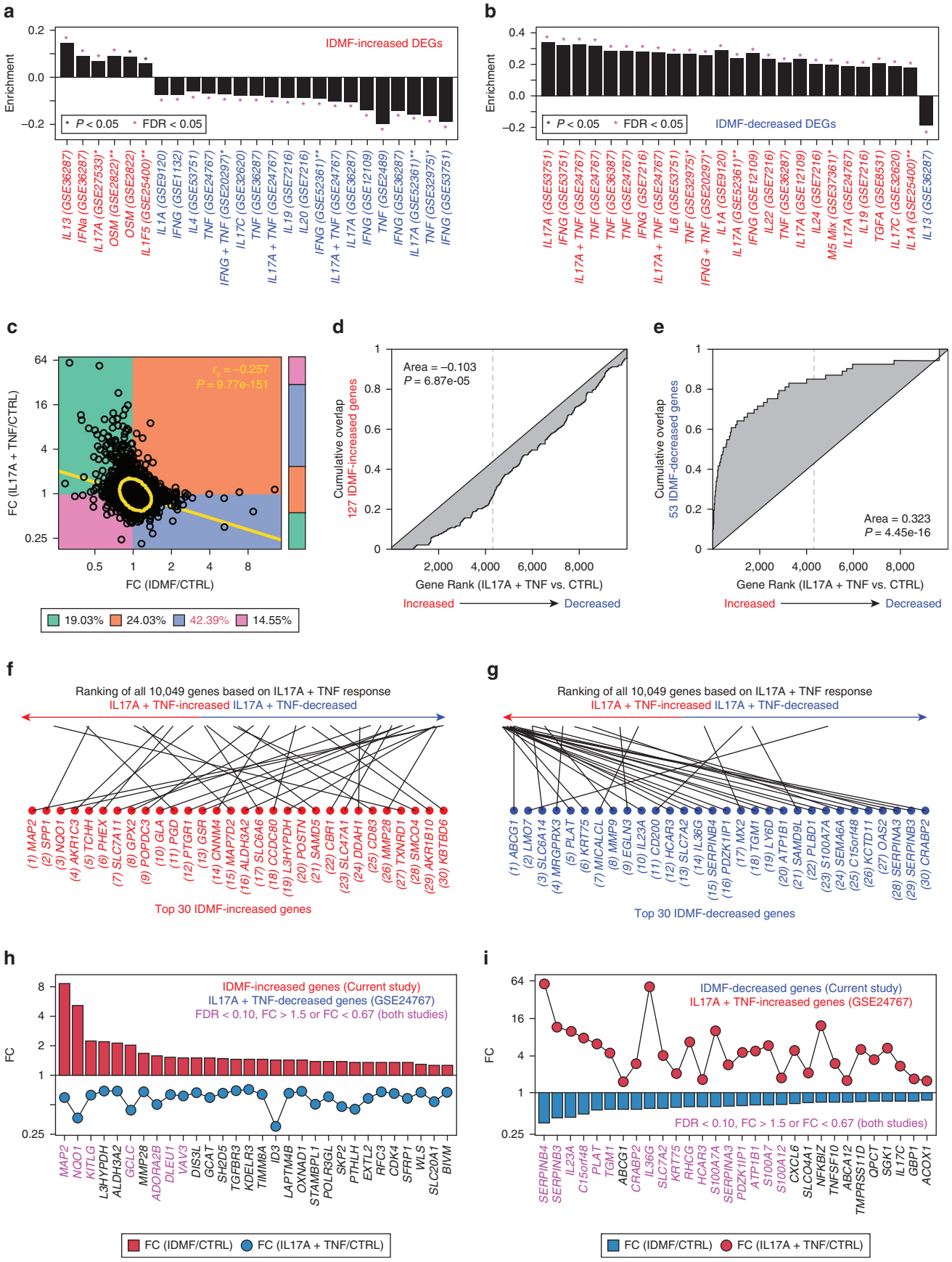

Figure 9. IDMF versus cytokine signatures. (**a, b**) Cytokine signatures associated with (**a**) IDMF-increased and (**b**) IDMF-decreased DEGs. Enrichment indicates bias toward cytokine-increased (>0, red label) or cytokine-decreased (<0, blue label) expression (experiments performed with KCs; *HaCaT, **RHE). (**c**) FC

Oxidative stress is postulated to play an important role in psoriasis lesion development (Kadam et al., 2010). Within psoriasis lesions, accumulation of oxidative stress is partly due to neutrophils, which undergo respiratory bursts to release superoxide anion (Chiang et al., 2019). Activation of the NRF2–ARE pathway is thus thought to be an important mechanism underlying the antipsoriatic effects of DMF (Brück et al., 2018). For example, DMF and/or MMF activates NRF2 in KCs (Helwa et al., 2017; Lee et al., 2017; Li et al., 2018) and represses NRF2 and its target genes in psoriasis lesions (Lee et al., 2017). On the basis of luciferase gene assays, IDMF was a stronger activator of NRF2 than DMF (Figure 12), and IDMF upregulated multiple genes linked to oxidative stress response and GSH metabolism (Figure 7g and i). IDMF may thus share antioxidant mechanisms with DMF and MMF, but with topical application, IDMF may act directly on ROS generated by epidermal neutrophils (Chiang et al., 2019).

The application of IMQ to elicit psoriasiform lesions in mice has been used as a practical model for evaluating the antipsoriatic effects of compounds and for a better understanding of the underlying disease mechanisms (Chuang et al., 2018). In this study, IDMF significantly reduced erythema, scaling, and epidermal thickness of IMQ-induced lesions (Figure 13b–13d), with repression of genes having elevated expression in such lesions (Figure 14c) as well as genes associated with immune activation (Figure 14f). We did not concurrently evaluate the effects of DMF in mouse IMQ–induced lesions because previous work has established that DMF elicits cutaneous sensitizing reactions in human and animal skin (Gehring and Gloor, 1990; Lahti and Maibach, 1985) and lesional skin from patients with psoriasis (Nieboer et al., 1989). Nonetheless, direct comparisons between topically applied fumarate compounds, such as IDMF and DMF, may be valuable for future work to understand the trade-offs between sensitization and antipsoriatic efficacy.

These data show that IDMF—a derivative of the antipsoriasis drug DMF—has DMF-like antipsoriatic activity without skin sensitization. This creates an opportunity to develop a treatment strategy on the basis of the DMF mechanism of action, but applied topically, to permit direct action on KCs and to circumvent systemic side effects of orally administered DMF (Reszke and Szepietowski, 2020). Finally, whereas most new antipsoriatic actives have focused on immunomodulation, our data suggest a unique pleiotropic mechanism of IDMF that involves dual anti-inflammatory and antioxidant effects.

MATERIALS AND METHODS

In silico simulation of DMF and IDMF transition energies

The ground state molecular structure of GSH and the alkene group (C=C) of DMF and IDMF were subjected to density functional theory with calculations to determine the bond-forming and -breaking mechanism. The B3LYP functional was used in conjunction with the 6-31+G(d,p) basis set. The structures were optimized, and frequency calculations were performed on the optimized structures to confirm only one negative frequency. The minimum reaction energy path was then determined by the intrinsic reaction coordinate calculation (Gonzalez and Schlegel, 1990, 1989). Structures for the reactant, transition state, and product were obtained, and single-point calculations were used to determine relative energy and kinetic parameters. All calculations were performed using Gaussian 09 (Wallingford, CT; Frisch et al., 2009).

Fatty acid ester hydrolysis with CES2

DMF (1 mM) or IDMF (1 mM) was dissolved in 2% DMSO and 10% ethylene glycol in 20 mM 4-(2-hydroxyethyl)-1-piperazineethanesulfonic acid at a pH of 7.4. We then added 20 μl of CES2 enzyme (1 mg/ml) and incubated at 37 °C for 30, 60, 120, and 240 minutes. The reaction was stopped using methanol. DMF, IDMF, and isosorbide MMF were quantified using a UV detector at 210 nm. Isosorbide was quantified using charged aerosol detection. The weak solvent was 0.1% formic acid in water, whereas the strong solvent was methanol. For the DMF analysis, the Kinetex C18 4.6 × 100 mm column was used (2.6μ, Phenomenex, Torrance, CA) with a flow rate of 0.45 ml/min. For the IDMF analysis, the Luna C18 4.6 × 100 mm column was used (5μ, Phenomenex) with a flow rate of 1.0 ml/min.

Phototoxicity assays

Neutral red uptake phototoxicity assays were performed on the basis of the Organisation for Economic Co-operation and Development guidelines with chlorpromazine as a positive control (Ates et al., 2017). Two 96-well plates were seeded with normal neonatal human dermal fibroblasts (catalog number 106-05n; Cell Applications, San Diego, CA) at 15,000 cells per well in DMEM supplemented with 10% calf serum. Cells were grown overnight in a humidified atmosphere at 37 °C in 5% carbon dioxide. Test materials (water negative control, chlorpromazine positive control, and IDMF) were added to both plates in Hank's Balanced Salt Solution. Cells were then returned to an incubator for 1 hour. One plate was then placed in the dark at room temperature, whereas the other (identical) plate was irradiated through the lid with UVA using a UVA-28T (UltraLum, Claremont, CA) lamp (5 J/cm^2). After UVA irradiation, the medium with test materials was removed from both plates and replaced by a fresh cell culture medium. Plates were then returned to the incubator for 24 hours. After this time, the medium was replaced with a neutral red medium (50 mcg/ml), and cells were incubated for 3 more hours. Wells were then washed with Hanks Balanced Salt Solution, and neutral red was extracted from cells with a solution consisting of 1.0% glacial acetic acid, 50% ethanol, and 49% water. After a 30-minute extraction with mixing, the absorbance of each well was measured at 570 nm using the Bio-Rad 3550-UV microplate spectrophotometer (Bio-Rad Laboratories, Hercules, CA). To assess phototoxicity, average neutral red uptake was compared between UVA(–) and UVA(+) cells at the same MMF or IDMF concentration (Fisher's least significant difference).

Ames genotoxicity assays

The *Salmonella* mutagenicity test kit was obtained from Molecular Toxicology (Boone, NC) (Maron and Ames, 1983; Mortelmans and

scatterplot. IDMF versus IL17A + TNF response (GSE24767, n = 3 per group) (top: proportion of genes/quadrant; red: $P < 0.05$, Fisher's exact test). (**d, e**) GSEA. Area between the overlap curve and diagonal is shown (>0: DEGs enriched among IL17A + TNF–increased genes; <0: DEGs enriched among IL17A + TNF–decreased genes). (**f, g**) Top 30 IDMF-increased/-decreased genes (bottom) and their positions within a list of 10,049 genes ranked on the basis of IL17A + TNF response (GSE24767). (**h**) IDMF-increased/IL17A + TNF–decreased genes. (**i**) IDMF-decreased/IL17A + TNF–increased genes. CTRL, control; DEG, differentially expressed gene; FC, fold change; GSEA, Gene Set Enrichment Analysis; IDMF, isosorbide di-(methyl fumarate); KC, keratinocyte; RHE, reconstituted human epidermis.

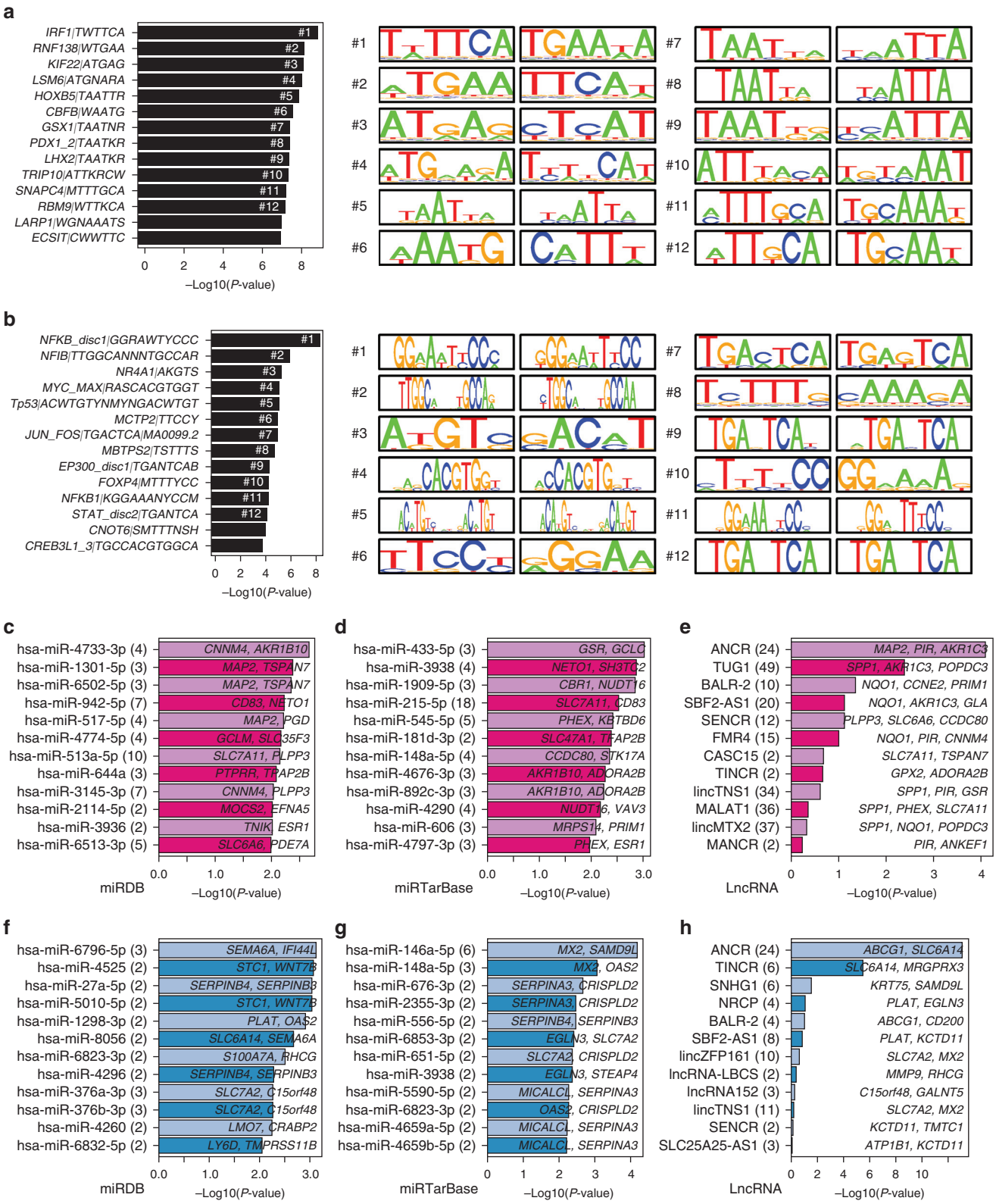

Figure 10. TF binding sites, microRNAs, and lncRNAs associated with IDMF-altered DEGs. (**a, b**) TF binding sites associated with (**a**) IDMF-increased and (**b**) IDMF-decreased DEGs. Sequence logos for the top-ranked 12 binding sites are shown (from among 2,935 motifs screened). Enrichment of binding sites in the 5 kb upstream region of DEGs was evaluated (*P*-values: semiparametric generalized additive logistic models). (**c, f**) MicroRNAs with target genes from the miRDB database enriched among (**c**) IDMF-increased DEGs and (**f**) IDMF-decreased DEGs. (**d, g**) MicroRNAs with target genes from the miRTarBase enriched among (**d**) IDMF-increased and (**g**) IDMF-decreased DEGs. (**e, h**) LncRNAs from the LncRNA2Target database enriched among (**e**) IDMF-increased and (**h**) IDMF-decreased DEGs. In **c–h**, the number of DEGs associated with each microRNA or lncRNA is shown (parentheses), and exemplar target DEGs are listed on the corresponding row within each figure (*P*-values: Fisher's exact test). All analyses in **a–h** were performed on the

Zeiger, 2000). This MOLTOX assay (catalog number 31-100-2) contains two *Salmonella typhimurium* strains (TA1535 and TA1537) carrying different mutations of histidine synthesis genes. Assays were completed following the manufacturer's instructions. Colony counts were $\log_{10}$-transformed for statistical analysis. Mutagenicity was assessed by comparing the average count between IDMF- and water-treated (control) organisms (two-sample two-tailed *t*-test).

Effect of DMF and IDMF on CPD repair

Adult human dermal fibroblasts (low passage, Zen-Bio, Research Triangle, NC; catalog number DF-F) were grown in DMEM/10% fetal bovine serum without phenol red indicator until cells reached a subconfluent state. Cells were then starved in a serum-free DMEM medium containing 10% Cell-Ess without GFs (Essential Pharmaceuticals, Newtown, PA) overnight, incubated with test materials, and irradiated the following day (after 24 hours of contact with test materials) with a Spectronics UVA lamp (Spectronics, Melville, NY) (without lid) for 3.75 hours at 76 J/cm^2 (except for nonirradiated CTRLs) (Besaratinia et al., 2005). Immediately after irradiation, cells were returned to the incubator for 3 hours to allow CPD repair. CPDs were quantified using the Cyclex Cellular UV DNA Damage Detection Kit (catalog number CY-1141) from MBL International (Woburn, MA) following the Cyclex protocol (version number 120420). The colorimetric reaction was terminated using the stopping solution (1N sulphuric acid), and the signal proportional to CPD amount was read at 450 nm using the SpectraMax 190 Microplate Reader from Molecular Devices. Each experimental condition was tested in three biological replicates. Signals were normalized to the water control treatment, and comparisons among treatments were made using Fisher's least significant difference test.

Mouse tail skin testing

Laboratory studies of mouse tail skin were done in compliance with the United States Public Health Service (PHS) policy on the humane care and use of laboratory animals with approval obtained from the United States National Institutes of Health Office of Laboratory Animal Welfare (OLAW) (animal welfare assurance no. A7861-01). Male albino (BALB/c) mice aged 5–7 weeks (The Jackson Laboratory, Bar Harbor, ME) were randomly divided into groups of four mice each. Using a glove-protected finger, each mouse was treated down to 1 cm below the proximal half of the tail once daily (5 days per week) for a total of 13 days with 100 mg of IDMF or Tazarotec gel (0.1%, Allergan, Dublin, Ireland) as a positive control. IDMF (2%) was formulated in a pharmaceutically acceptable cream with penetration enhancer dimethyl isosorbide, butylene glycol, and glycerin. Untreated tails were used as the negative control. On day 14, mice were killed, and the proximal half of tails were cut, transversely sectioned, and preserved in 10% formalin for histochemical evaluation.

Acute dermal toxicity study of IDMF in rats

This study was performed to assess the acute dermal toxicity of IDMF after a single dermal exposure with the goal of recommending a Globally Harmonized System of Classification and Labeling of Chemicals category (Pratt, 2002). The study was conducted in full compliance with the Organisation for Economic Co-operation and Development principles of good laboratory practice. The study was further compliant with guidelines issued by the International Association for Assessment and Accreditation of Laboratory Animal Care. The project proposal for experimentation was approved by the Institutional Animal Ethics Committee of the Jai Research Foundation (Vapi, India).

The study used five nulliparous and nonpregnant female rats (*Rattus norvegicus*) aged 11–15 weeks. Rats were housed in polypropylene cages covered with stainless steel grid tops with autoclaved clean rice husk used as bedding material. Wooden blocks were provided as enrichment material. Each cage was supplied with a polypropylene water bottle and stainless steel nozzle. Rats were housed three per cage except on the day of IDMF application. Rats were housed individually after IDMF application before patch removal. Each rat was uniquely numbered on the tail using a tattoo machine on day 1. Rats were provided ad libitum access to Teklad-certified feed (Envigo, Indianapolis, IN) and UV-sterilized reverse osmosis filtered water. Rats were maintained at room temperature (19–23 °C) with 56–66% relative humidity. A fixed photoperiod was maintained using an automatic timer with 12 hours of artificial light and 12 hours of darkness.

The fur of each test subject was closely clipped from the dorsal area of the trunk using an electric clipper without abrading or damaging the skin. More than 10% of the body surface area was clipped approximately 24 hours before IDMF application. A starting IDMF dose of 200 mg/kg was selected. Three rats were used in a dose-finding study, and two were used for the main experiment. Rats in the dose-finding study were treated with 200, 1,000, and 2,000 mg/kg, with a single dermal application sequentially and a minimum gap of 48 hours. According to the observations from this study, two additional rats were tested sequentially at 2,000 mg/kg. The required amount of IDMF based on weight was applied over the clipped area (approximately 7 cm × 5 cm) and remained in contact with the skin for 24 hours. The applied IDMF was held in contact with skin using a porous gauze dressing (8 ply or less) and nonirritating hypoallergenic surgical tape (Medi tape 330). This dressing prevented any loss of the test item and ensured that rats did not lick or ingest it. After the 24-hour exposure period, the residual IDMF was removed using cotton soaked in reverse osmosis water.

Rats were observed for signs of toxicity and mortality within 0.5 hours and at 2, 4, and 6 hours after dermal application on the day of dosing (day 0). Subsequently, rats were observed twice daily for morbidity and mortality for 14 days. Erythema and edema were recorded at 24, 48, and 72 hours after patch removal. Clinical signs were recorded once a day. Individual body weight was recorded before dermal application on day 0 and on days 7 and 14 after dermal application. At the end of the 14-day observation period, all rats were killed by carbon dioxide asphyxiation and were subjected to gross pathological examination, consisting of external examination and opening of abdominal and thoracic cavities.

Acute dermal irritation study of IDMF in rabbits

This study was performed to assess the acute dermal irritation potential of IDMF in rabbits. The study was conducted in compliance with the Organisation for Economic Co-operation and Development principles of good laboratory practice as well as with the

basis of 140 IDMF-increased DEGs (FDR < 0.10 with FC > 1.50) or 56 IDMF-decreased DEGs (FDR < 0.10 with FC < 0.67). DEG, differentially expressed gene; FC, fold change; FDR, false discovery ratio; IDMF, isosorbide di-(methyl fumarate); kb, kilobase; lncRNA, long noncoding RNA; TF, transcription factor.

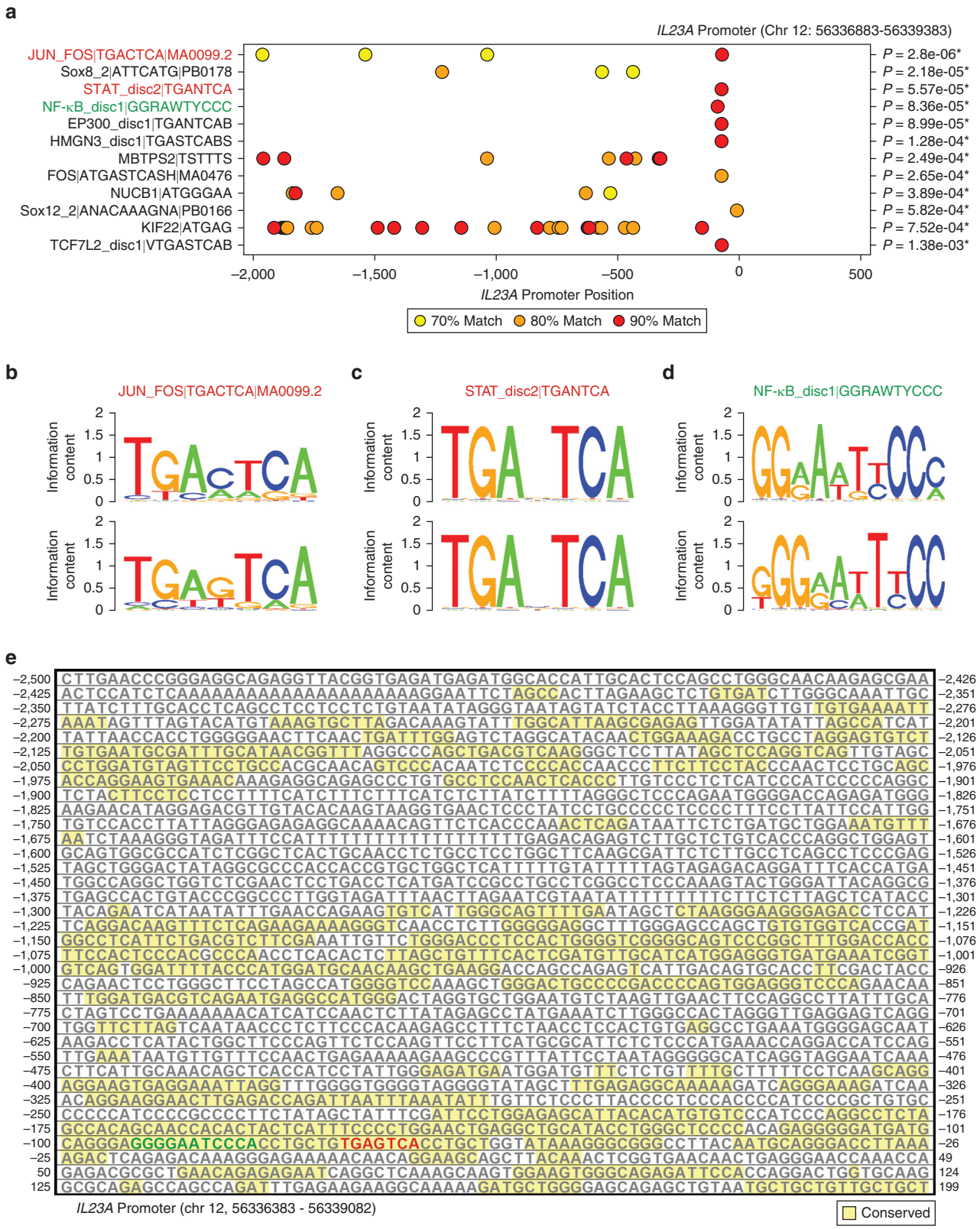

Figure 11. TF binding sites enriched in the *IL23A* promoter. (**a**) The top-ranked motif matches are shown within the *IL23A* promoter sequence (interval: −2 kb and 0.5 kb). Matches are shown at three levels of stringency (70% = weakest match; 90% = strongest match). The enrichment of motifs in the 2 kb upstream region of IDMF-decreased DEGs (FDR < 0.10 with FC < 0.67) is indicated by *P*-values derived from semiparametric generalized additive logistic models (right margin). (**b–d**) Sequence logos associated with the AP-1 (JUN-FOS), STAT, and NF-κB motifs shown in **a**. (**e**) The *IL23A* promoter sequence is shown with AP-1/STAT (red) and NF-κB binding sites (green). Conserved sequences (PhastCons ≥ 0.20) are highlighted (yellow). AP-1, activated protein-1; Chr, chromosome; DEG, differentially expressed gene; FC, fold change; IDMF, isosorbide di-(methyl fumarate); kb, kilobase; STAT, signal transducer and activator of transcription; TF, transcription factor.

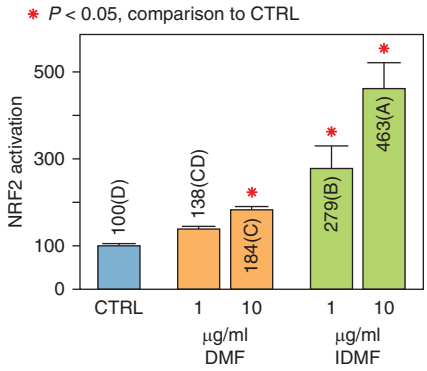

Figure 12. Effect of DMF and IDMF on NRF2-mediated gene expression (luciferase assays). ARE-transfected HEK293 cells were treated with IDMF for 24 hours, and NRF2 activation was measured using luciferase assays. The vertical axis shows NRF2 activation quantified using firefly/renilla ratios normalized to the CTRL treatment (n = 3–6 replicates per group). The mean normalized ratio is shown for each group (±1 standard error). Groups sharing the same letter do not differ significantly ($P > 0.05$, Fisher's LSD). A red asterisk is used to denote a significant difference compared with the CTRL treatment (*$P < 0.05$, Fisher's LSD). ARE, antioxidant response element; CTRL, control; DMF, dimethyl fumarate; HEK293, human embryonic kidney 293; IDMF, isosorbide di-(methyl fumarate); LSD, least significant difference.

Table 1. IDMF (5%) and Placebo Lotions (IMQ Mouse Study)

INCI Name	Trade Name (Supplier)	Phase	IDMF Lotion[1]	Placebo[2]
Water (demineralized)	NA	A	Qs	Qs
Disodium EDTA	NA	A	0.1	0.1
Glycerin	Glycerin 99% (Ruger)	A	2	2
Butylene glycol	Butylene Glycol (Ruger)	A	2	2
Xanthan gum	Rhodicare S (Rhodia)	A-1	0.1	0.1
Acrylates/C10–30 alkyl acrylate crosspolymer	Carbopol Ultrez 21 (Lubrizol)	A-1	0.25	0.25
Caprylic/capric triglycerides	Myritol 318 (Cognis)	B	4	6
Mineral oil, lanolin alcohols	Fancol LAO (Elementis)	B	2	2
Oleth-10	Brij-10 (Croda)	B	0.5	0.5
Glyceryl stearate, PEG-100 stearate	Arlacel 165 (Croda)	B	2.5	2.5
Dimethicone	DC, 200/100CST (Dow Corning)	B	2	3
Stearic acid	Stearic Acid, NF/ Spectrum (Spectrum Chemical)	B	1	1
Cetyl alcohol	Crodacol C-70 (Croda)	B	1.5	1.5
Triethanolamine	Triethanolamine 99%	C	0.15	0.15
Dimethyl isosorbide	Arlasolve DMI (Croda)	D	15	15
IDMF	IDMF (Symbionyx)	D	5	0
Phenoxyethanol, ethylhexylglycerine	Euxyl 9010 (Schulke)	E	1	1
Total			100	100

Abbreviations: cps, centipoise; IDMF, isosorbide di-(methyl fumarate); INCI, international nomenclature cosmetic ingredient; NA, not applicable; Qs, as much as is sufficient; sp, surface poise.

The table lists the INCI ingredient name, trade name (with supplier), and phase. The final two columns list the weight concentration (% w/w) for the IDMF and placebo lotions, respectively.

[1]Combine phase A; disperse A2 in A1 while stirring and heat A to 75 °C and begin heating to 75 °C. Combine phase B ingredients, and then, heat the mixture to 75 °C. Add phase B to A with good mixing. Add phase C and premixed D. Homogenize mixture at moderate speed while cooling to ~40 °C. Add preservative and stir homogeneously until uniform. pH = 6.0. Viscosity = 30,000–40,000 cps (sp 4, 5 r.p.m.).

[2]Combine phase A; disperse A1 while stirring and heat A to 75 °C. Combine phase B ingredients, and then, heat the mixture to 75 °C. Add phase B to A with good mixing. Neutralize with phase C. Homogenize mixture and add phase D at ~50 °C. Add phase E and preservative and stir homogeneously until uniform. pH = 6.0. Viscosity = 30,000–40,000 cps (sp 4, 5 r.p.m.)

International Association for Assessment and Accreditation of Laboratory Animal Care guidelines. The project proposal was approved by the Institutional Animal Ethics Committee of the Jai Research Foundation.

The study was performed using male New Zealand White rabbits (*Oryctolagus cuniculus*) aged 13–14 weeks (n = 3). Rabbits were individually housed in stainless steel wire mesh cages, with each cage having a polypropylene water bottle and stainless steel nozzle. A rabbit rattle was provided as enrichment material. Each rabbit was uniquely numbered on the ear using a tattoo machine on day 1. Rabbits were provided with ad libitum access to Teklad-certified feed (Envigo) and UV-sterilized water filtered by reverse osmosis. Rabbits were housed at room temperature (18–22 °C) at 63–65% relative humidity, with a fixed photoperiod maintained using an automatic timer (12 hours light, 12 hours darkness). Only rabbits with healthy intact skin were selected for the study.

Fur was removed from the dorsal region at four contralateral sites for rabbit 1 and two contralateral sites for rabbits 2 and 3. Care was taken not to abrade the skin. An area >6 cm^2 was clipped at both sites approximately 24 hours before treatment. A 500 mg dose of IDMF (moistened with 0.5 ml distilled water) was applied evenly and sequentially to three of the clipped sites of rabbit 1. Patches were then removed using distilled water after 3 minutes, 1 hour, and 4 hours. The 3-minute and 1-hour test sites were evaluated for skin irritation immediately after patch removal. Subsequent evaluations were performed 1, 24, 48, and 72 hours after removal of the 4-hour patch. Because no severe irritation was observed at any test site in rabbit 1, two additional rabbits were tested simultaneously. IDMF was applied to one of the clipped sites of rabbits 2 and 3 for 4 hours using the same method described earlier. The other contralateral clipped site of each rabbit remained untreated and served as the control site.

Treated and control sites were covered with gauze patches of approximately 6 cm^2 and secured at the margins by nonirritating hypoallergenic surgical tape (Medi tape 330). At the end of the appropriate exposure period (3 minutes, 1 hour, and 4 hours) (day 0), residual IDMF was removed with cotton soaked in distilled water. Detailed clinical signs were recorded once a day, and rabbits were observed for morbidity and mortality twice daily. Body weights were recorded before the initiation of dosing and at the termination of the experiment. The 3-minute and 1-hour test sites were evaluated for skin irritation immediately after patch removal in rabbit 1. Skin reactions were observed 1, 24, 48, and 72 hours after patch removal.

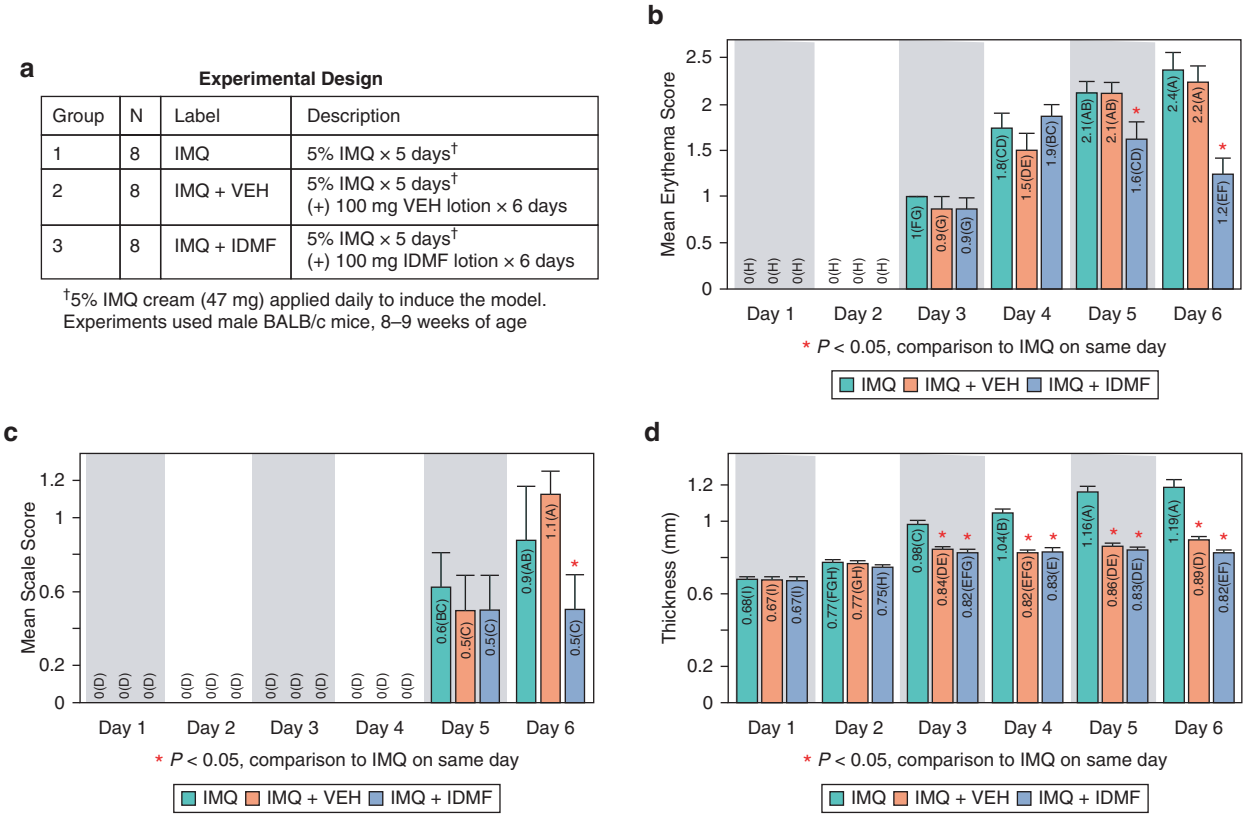

Figure 13. IDMF effect on IMQ-induced lesions. (**a**) Experimental design (n = 8 per group). (**b–d**) Skin erythema, scale, thickness. The average per group is shown (±1 SE). Treatments sharing the same letter do not differ significantly ($P > 0.05$, Fisher's LSD; *$P < 0.05$, IMQ comparison on same day). IDMF, isosorbide di-(methyl fumarate); IMQ, imiquimod; LSD, least significant difference; SE, standard error; VEH, vehicle.

The site of application was visually assessed and scored for erythema and edema. Rabbits were humanely killed by thiopentone sodium at the end of the observation period.

Skin sensitization study of IDMF in guinea pigs

This study was performed to determine the skin sensitization potential of IDMF in Hartley strain guinea pigs. The study was conducted in compliance with the Organisation for Economic Co-operation and Development principles of good laboratory practice and with the International Association for Assessment and Accreditation of Laboratory Animal Care guidelines. The project proposal was approved by the Institutional Animal Ethics Committee of the Jai Research Foundation.

Experiments were performed using Hartley strain guinea pigs (*Cavia porcellus*) that were aged 9–10 weeks (n = 30). The control group consisted of 10 guinea pigs, including 5 males and 5 females. The treatment group consisted of 20 guinea pigs, including 10 males and 10 females. Females were nulliparous and nonpregnant. The guinea pigs were received into the experimental room after veterinary examination and were allowed to acclimatize to laboratory conditions for 7 days before commencement of dosing. The guinea pigs were housed in polypropylene cages, with autoclaved clean corn cob used as bedding material. Each cage was supplied with a polypropylene water bottle with a stainless steel nozzle.

Individuals were identified by ear marks placed using a permanent ink marker before randomization. Unique number identifiers were placed on each individual using a tattoo machine after randomization. The guinea pigs were provided ad libitum access to Teklad-certified global high fiber guinea pig diet (Envigo) and UV-sterilized water filtered by reverse osmosis (supplemented with vitamin C at 1 g/l). Room temperature was maintained at 20–23 °C and 57–66% relative humidity. A fixed photoperiod was used with 12 hours of darkness and 12 hours of artificial light (06:00–18:00).

Pilot study and dose selection. Testing was performed to determine the highest concentration of IDMF required to produce mild skin irritation for induction and the highest nonirritating concentration for the main study challenge phase. IDMF was dissolved in a homogenous suspension of 80% ethyl alcohol and acetone. A patch loaded with 25, 50, 75, and 100 mg IDMF moistened with 0.2 ml 80% ethyl alcohol was topically applied to the clipped flanks of four guinea pigs (two males and two females). Patches were held in contact for 6 hours by an occlusive dressing (Medi tape 330). Skin reactions were evaluated 24 and 48 hours after patch removal following the Draize method (Draize, 1944). No skin reactions were observed. A total of 100 mg IDMF moistened with 0.2 ml of 80% ethyl alcohol was therefore selected for topical induction application on days 0, 7, and 14. Likewise, 100 mg IDMF moistened with 0.2 ml of acetone was selected for challenge application on day 28.

Buehler test. Testing was performed using 30 guinea pigs randomized into two groups as described earlier. Hair was removed from both flanks of guinea pigs using a clipper 24 hours before treatment for topical induction and challenge application.

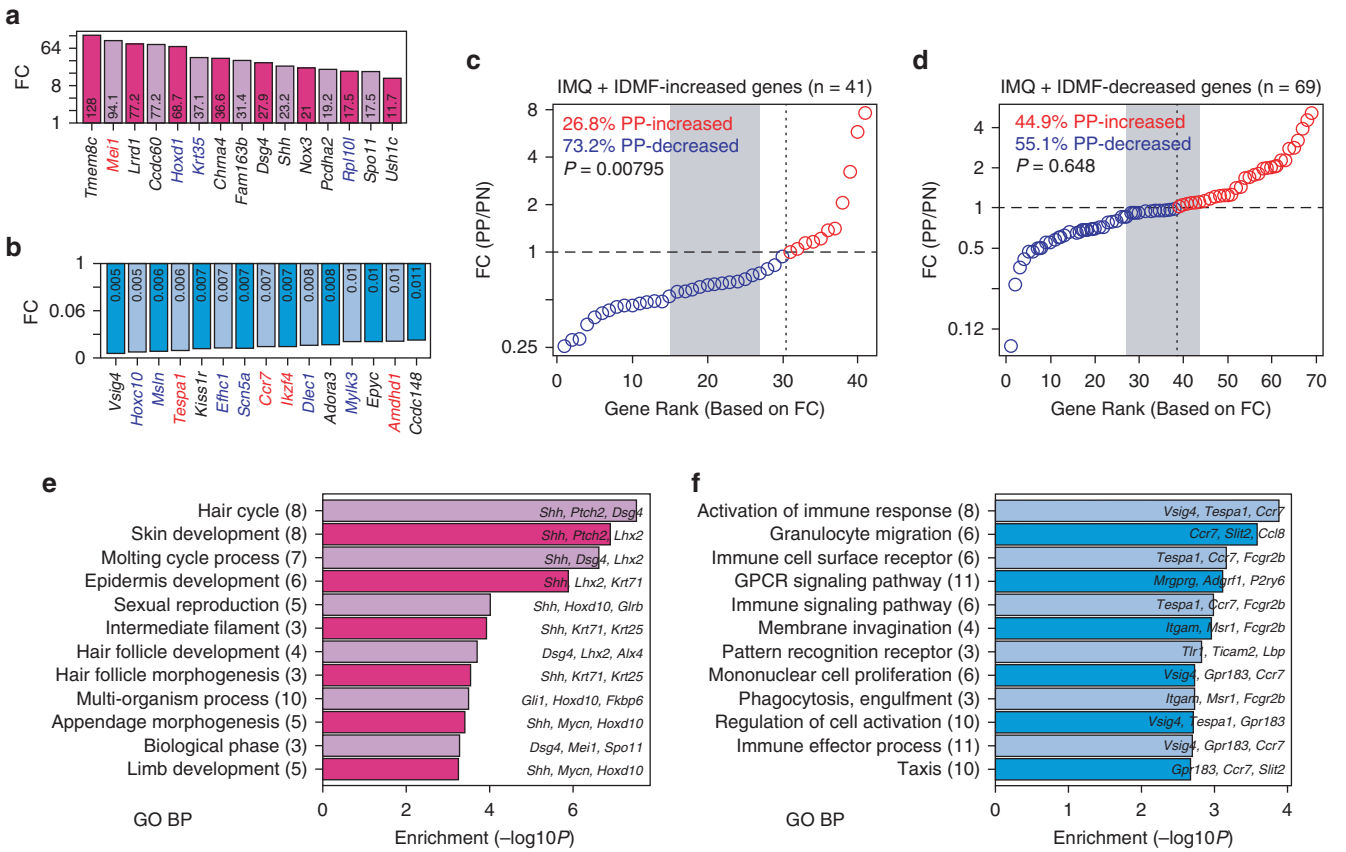

Figure 14. IDMF effect on IMQ-induced lesions (RNA-seq). The study was based on four independent biological replicates (IMQ, n = 1; IMQ + VEH, n = 2; IMQ + IDMF, n = 1). (**a**) IMQ + IDMF–increased and (**b**) IMQ + IDMF–decreased genes (red font: PP-increased; blue font: PP-decreased, RNA-seq meta-analysis). (**c, d**) FC estimates (PP/PN) for (**c**) IMQ + IDMF–increased and (**d**) IMQ + IDMF–decreased genes (vertical line: number of PP-decreased genes; gray: null hypothesis region; *P*-value was tested with Fisher's exact test). (**e, f**) GO BP terms enriched among (**e**) IMQ + IDMF–increased and (**f**) IMQ + IDMF–decreased genes (number of genes/term is given in parentheses; exemplar genes are listed within figures). BP, biological process; FC, fold change; GO, Gene Ontology; IDMF, isosorbide di-(methyl fumarate); IMQ, imiquimod; PN, uninvolved skin from psoriasis patient; PP, lesional skin from psoriasis patient; RNA-seq, RNA sequencing; VEH, vehicle.

Induction phase. In the treatment group (days 0, 7, 14), a nonirritating patch (4 cm × 2 cm) loaded with 100 mg IDMF moistened with 0.2 ml of 80% ethyl alcohol was applied to the left flank and held in contact by an occlusive dressing for 6 hours. Likewise, in the control group (days 0, 7, 14), a nonirritating patch (4 × 2 cm) loaded with 0.2 ml 80% ethyl alcohol was applied to the left flank and held in contact by an occlusive dressing for 6 hours. At the end of the exposure period, dressing and patch were discarded, and residual was removed using cotton soaked in distilled water. Skin reactions were evaluated 24 hours after patch removal on days 1, 8, and 15 following the Draize method (Draize, 1944).

Challenge phase (day 28, treatment and control groups). A nonirritating patch (4 × 2 cm) loaded with 100 mg IDMF moistened with 0.2 ml acetone was applied to the right flank of all guinea pigs. Patches were held in contact by an occlusive dressing for 6 hours. At the end of the exposure period, dressing and patch were discarded, and the residual test item was removed using cotton soaked in distilled water.

Observations. Guinea pigs were observed at least twice daily for morbidity and mortality. Clinical signs were recorded daily throughout the study. Skin reactions were evaluated 24 hours after patch removal on days 1, 8, and 15 following the Draize method (Draize, 1944). Skin reactions were evaluated 24 and 48 hours after patch removal on days 29 and 30. The initial (day 0) and terminal (day 30) body weight of guinea pigs was recorded. Guinea pigs were humanely killed at the end of the observation period by carbon dioxide asphyxiation.

Quality control analysis of Affymetrix microarray samples

Microarray studies were performed using the Affymetrix Human Genome U133 Plus 2.0 array platform, which includes 54,675 probeset features for assaying the expression of more than 47,000 transcripts. Hybridizations were performed by the University of Michigan Microarray Core Facility (Ann Arbor, MI) using the GeneChip 3′ IVT PLUS Reagent Kit (Thermo Fisher Scientific, Waltham, MA). Bioinformatic analyses were performed starting with raw CEL files returned by the core facility. Initial inspection of microarray pseudoimages did not identify prominent spatial artifacts to suggest problematic hybridizations (Figure 15a–d). The distribution of $\log_2$-scaled raw signal intensities for perfect match probes was similar among the four microarray samples (Figure 15e). The median normalized unscaled standard error was not significantly >1 for any array, and the normalized unscaled standard error interquartile range was similar among arrays and within acceptable limits (Figure 15f) (McCall et al., 2011). Likewise, the median relative log expression

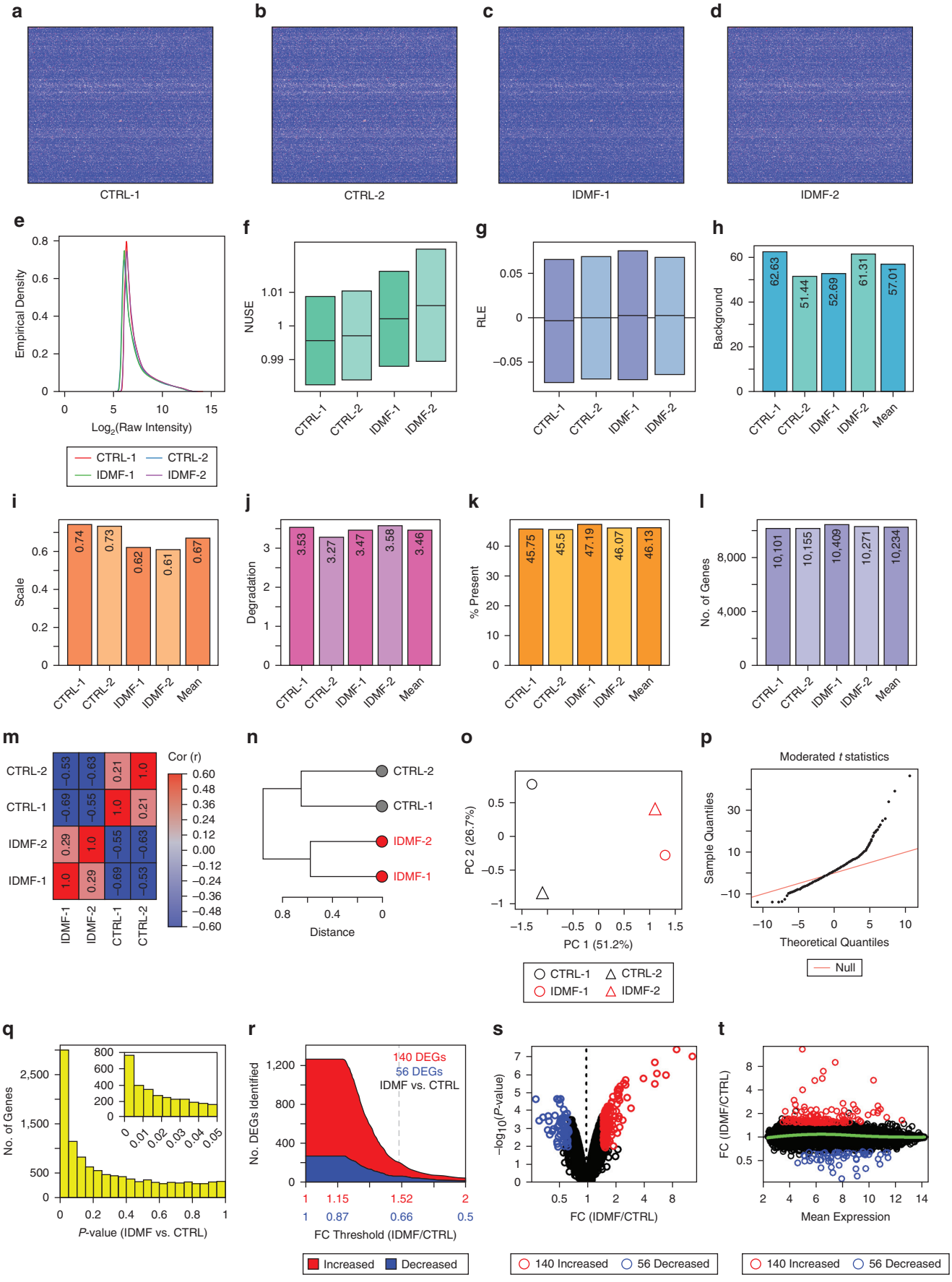

Figure 15. Microarray quality control and differential expression analysis (IDMF vs. CTRL). (**a–d**) Affymetrix array pseudoimages (n = 4 arrays). (**e**) Raw signal intensity distributions (604,258 probe signals per array). (**f**) NUSE. (**g**) RLE. In **f** and **g**, boxes outline the median and IQR for each array. (**h**) Average background.

was approximately zero for each array, and the relative log expression interquartile range was similar among arrays and within acceptable limits (Figure 15g) (McCall et al., 2011). Average background was similar among the four arrays to support similar efficiency of hybridization in each sample (Figure 15h). MicroArray Suite (MAS) 5.0 scale factors varied by not >25% among the samples, suggesting stability in the expression of most transcripts (Figure 15i). The slope measuring decay of signal intensities from the 3′ to 5′ end of transcripts (Atz et al., 2007) was similar among arrays and did not suggest high levels of RNA degradation (Figure 15j). An average of 46% of probe sets was called present on each array on the basis of comparison between corresponding perfect match and mismatch probe intensities, with similar percentage values in each of the four samples (range = 45.5–47.2%) (Figure 15k) (Liu et al., 2002).

Raw microarray data were normalized using the Robust Multichip Average algorithm to generate signal intensities on a $\log_2$ scale for 54,675 probe sets (Irizarry et al., 2003). These probe sets were filtered by choosing a single representative probe set for each of 20,161 human gene symbols. To choose a representative probe set, we preferentially selected those expected to hybridize specifically with their intended target (i.e., excluding those with _x_ or _s_ suffixes in their probe set identifier). A probe set with _x_ or _s_ suffix was only selected as a representative if no other probe sets were available for a given human gene. Otherwise, if multiple probe sets without an _x_ or _s_ suffix were available for the same gene, the probe set with the highest average expression among the four samples was chosen as a representative. This yielded a set of 20,161 nonredundant probe sets each associated with a distinct human gene. Of these, we selected 17,554 probe sets for which the associated human gene symbol corresponded to a protein-coding gene. Utilizing genome annotation available from Bioconductor (Gentleman et al., 2004), we considered protein-coding genes to be those associated with a UniProt protein identifier or a RefSeq transcript having an NM_ or NP_ prefix. Further analyses were performed utilizing these 17,554 probe sets associated with unique protein-coding genes. Only a fraction of these were expected to have a detectable expression in our experiments. A probe set was considered to have detectable expression if perfect match intensities were significantly above mismatch intensities ($P < 0.05$, Wilcoxon sign-rank test) (Liu et al., 2002). On the basis of this criterion, an average of 10,234 of the 17,554 probe sets (58.3%) had detectable expression in each of the four samples (Figure 15l).

Differential expression analysis (IDMF vs. CTRL)

To identify genes with an altered expression between IDMF and CTRL samples (n = 2 per treatment), differential expression tests were applied to 11,089 protein-coding genes having detectable expression in at least one of the four samples. Differential expression testing can be sensitive to outliers, but inspection of intersample correlation coefficients (Figure 15m), hierarchical cluster analysis of samples (Figure 15n), and a principal component scatterplot (Figure 15o) did not suggest evidence for outliers. Samples from the same treatment were also grouped together in unsupervised analyses (Figures 15n and 15o). Differential expression analysis was performed by fitting linear models to Robust Multichip Average–normalized signal intensities (R package: limma, function: lmFit), with *P*-values derived using *t*-statistics with the moderation of standard errors by an empirical Bayes method (R package: limma, function: eBayes) (Smyth, 2004). To control the FDR, raw *P*-values were adjusted using the Benjamini–Hochberg method (Benjamini and Hochberg, 1995).

A quantile–quantile plot of moderated *t*-statistics revealed an abundance of low and high *t*-statistics, suggesting significant differential expression for a fraction of genes analyzed (Figure 15p). Consistent with this, the raw *P*-value distribution was nonuniform with an abundance of genes having low *P*-values (Figure 15q). Without applying an FC threshold, 1,269 genes would have been identified as differentially expressed with FDR < 0.10 (1,004 IDMF-increased DEGs, 265 IDMF-decreased DEGs) (Figure 15r). A conservative FC threshold > 1.50 or < 0.67 was applied in addition to the FDR < 0.10 criterion, yielding 196 IDMF-altered DEGs (140 IDMF-increased DEGs, 56 IDMF-decreased DEGs) (Figure 15r). A volcano plot showed reasonable symmetry of increased and decreased FC estimates (Figure 15s), and an MA plot did not reveal bias of FC estimates among genes having low or high expression (Figure 15t).

Gene annotation enrichment and motif analyses

The gene annotations enriched among IDMF-increased/-decreased DEGs were identified using the Gene Ontology and Kyoto Encyclopedia of Genes and Genomes databases (Gene Ontology Consortium et al., 2013; Kanehisa et al., 2016). Enrichment of DEG annotations relative to the background set of 11,089 KC-expressed genes included in differential expression analyses was evaluated using a conditional hypergeometric test (R package: GOstats; function: hyperGTest) (Falcon and Gentleman, 2007). Semiparametric generalized additive logistic models were used to identify motifs enriched in 2 kilobase and 5 kilobase regions upstream of DEG transcription start sites (Swindell et al., 2013). These analyses were performed using a set of 2,935 empirically determined DNA motifs associated with human transcription factors or unconventional DNA binding proteins (Swindell et al., 2015b).

(**i**) MAS 5.0 algorithm scale factors. (**j**) RNA degradation score. The score calculated for each array represents the decay of signal intensities from the 3′ to 5′ end of probe sets. (**k**) Percentage of probe sets called present per array (based on a comparison between perfect match and mismatch probes). (**l**) No. of protein-coding genes detected per array (Wilcoxon signed-rank, $P < 0.05$). The expression of 17,554 protein-coding genes was assayed after having applied all probe set filtering criteria. In **h–l**, the value obtained for each array is shown along with the average among all the four arrays. (**m**) Intersample Spearman correlation estimates. Correlations were calculated on the basis of mean-adjusted RMA signal intensities. (**n**) Sample clustering. Hierarchical clustering was performed on normalized and scaled signal intensities using average linkage and the Euclidean distance. (**o**) PC plot. The four samples are plotted with respect to the first two PC axes. (**p**) Moderated *t*-statistic quantile–quantile plot. Each point represents an individual protein-coding gene. Points off the red line are consistent with differential expression. (**q**) Differential expression *P*-value distribution. (**r**) No. of DEGs detected as a function of selected FC threshold. The dotted line represents the selected thresholds of FC > 1.50 and FC < 0.67. (**s**) Volcano plot. (**t**) MA plot. In **s** and **t**, DEGs are represented by red and blue symbols (FDR < 0.10 with FC > 1.50 or FC < 0.67). Analyses shown in **m–t** are based on the expression of 11,089 protein-coding genes with expression detected in at least one of the four samples. Cor, correlation; CTRL, control; DEG, differentially expressed gene; FC, fold change; FDR, false discovery ratio; IDMF, isosorbide di-(methyl fumarate); IQR, interquartile range; MAS, MicroArray Suite; No., number; NUSE, Normalized Unscaled Standard Error; PC, principal component; RLE, Relative Log Expression; RMA, Robust Multichip Average.

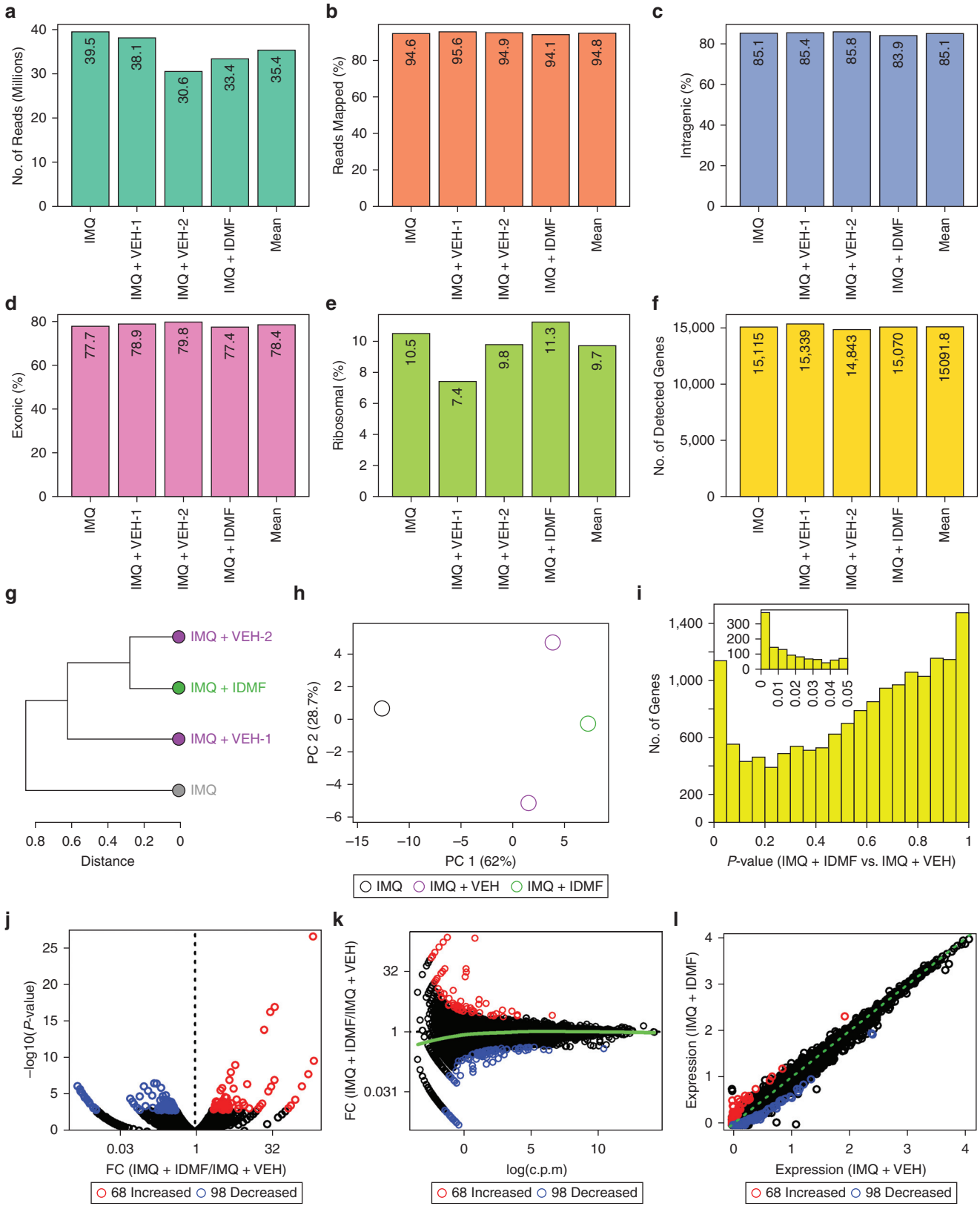

Figure 16. Microarray QC and differential expression analysis (IMQ + VEH vs. IMQ + IDMF). (**a**) Number of reads per sample after QC filtering. (**b**) Percentage of mapped reads. (**c**) Percentage of reads mapped to intragenic regions. (**d**) Percentage of reads mapped to exons. (**e**) Percentage of reads mapped to ribosomal RNA. (**f**) No. of protein-coding genes detected in each sample. (**g**) Cluster analysis. Hierarchical clustering was performed using average linkage and the Euclidean distance. (**h**) PCs plot. The four samples are plotted with respect to the first two PC axes. In **g** and h, analyses were performed on the basis of the expression of 15,927 protein-coding genes with detectable expression in at least one of the four samples. (**i**) Differential expression analysis raw *P*-value distribution (IMQ + IDMF vs. IMQ + VEH). The inset shows the left tail of the distribution ($P < 0.05$). (**j**) Volcano plot. The $\log_{10}$-transformed *P*-value from the differential expression analysis is plotted with respect to the FC estimate. (**k**) MA plot. The FC estimate is plotted with respect to the average abundance measured

NRF2-responsive ARE reporter assay

The ARE reporter assay is a mixture of two components. The first component is an NRF2-responsive luciferase construct encoding the firefly luciferase reporter gene under the control of an mCMV promoter and tandem repeats of the ARE transcriptional response element. The second component is a constitutively expressing renilla element (40:1), which acts as an internal control for normalizing transfection efficiencies and monitoring cell viability. Human embryonic kidney 293 cells (Sigma-Aldrich, St. Louis, MO; catalog number 85120602) were seeded at 50,000 per well in 96-well white opaque-wall tissue culture plates. Cells were transfected by mixing Cignal reporter assay firefly/renilla luciferase constructs (catalog number CCS-5020L; Qiagen, Germantown, MD) with Attractene Transfection Reagent (Qiagen) in Opti-MEM (Thermo Fisher Scientific) supplemented with 1% MEM nonessential amino acid solution without L-glutamine (Sigma-Aldrich; catalog number M7145). Test materials were added after media change, and their effect on NRF2 induction was quantified 24 hours later using the dual-luciferase reporter assay system (catalog number E1960; Promega, Madison, WI). Signal quantification was obtained using the DLReady validated Thermo Fisher Scientific Luminoskan Ascent Microplate Luminometer.

Effects of IDMF on IMQ-induced psoriasiform lesions in mice

The effect of IDMF on IMQ-induced lesions was evaluated in experiments performed by Charles River Laboratories (Montreal, Canada). The protocol and procedures involving the care and use of animals in this study was reviewed and approved by the Charles River Montreal (CR-MTL) Institutional Animal Care and Use Committee (IACUC). During the study, the care and use of animals were conducted in accordance with guidelines of the United States National Research Council (NRC) and the Canadian Council on Animal Care (CCAC).

Male BALB/c mice aged 8–9 weeks (Charles River Laboratories) received daily topical application of 5% IMQ cream on back skin for 5 consecutive days to induce lesional skin formation. IMQ cream (47 mg) was applied daily to an area 4 × 2 cm in size. Mice were divided into three groups of eight mice each (IMQ only, IMQ + VEH, IMQ + IDMF) (Figure 13a). The IMQ group received only IMQ without VEH or IDMF lotions. In the IMQ + VEH and IMQ + IDMF groups, VEH and IDMF lotions (100 mg) (Table 1) were applied, respectively, about 1 hour after IMQ application on each day of the experiment. Daily in-life measurements of the treatment area were performed to assess erythema, scaling, and skin thickness. Erythema was scored using a red color scale and a five-point scale (0 = none, 1 = slightly red, 2 = moderately red, 3 = markedly red, 4 = very markedly red). Scaling was likewise graded using a five-point scale (0 = none, 1 = slightly scaly, 2 = moderately scaly, 3 = markedly scaly, 4 = very markedly scaly). Back skin thickness was measured using an engineering micrometer, with measurements taken in the test region by folding treated skin between thumb and index fingers. On day 6, mice were killed, and terminal back skin samples were collected for RNA extraction.

The RNA-seq study was performed using four independent biological replicates (IMQ, n = 1; IMQ + VEH, n = 2; IMQ + IDMF, n = 1). Single-end 50-cycle cDNA sequencing (HiSeq 2000, Illumina, San Diego, CA) was performed by the University of Michigan Sequencing Core Facility. FastQC was used for quality assessment of raw fastq files (Brown et al., 2017). Adaptor removal and read quality filtering were performed using the cutadapt algorithm (Martin, 2011) and FastX toolkit (Hannon, 2010). Reads were mapped to the mouse (GRCm38/mm10) genome using the tophat2 algorithm with default settings (Kim et al., 2013). Fragments per kilobase million and fragments per kilobase million confidence intervals were calculated using Cufflinks (Trapnell et al., 2012). Raw gene counts for differential expression analysis were computed using the HTseq library (Anders et al., 2015). Postmapping quality control assessment of alignment files was performed using the RSeQC (Wang et al., 2012) and RNA-SeQC (DeLuca et al., 2012) software.

An average of 35.4 million reads per sample were obtained after quality control filtering (Figure 16a). Of these, 94.8% of the quality-filtered reads were mapped to the mm10 genome (Figure 16b), with 85.1% mapped to intragenic regions and 78.4% mapped to exonic regions (Figure 16d). Fewer than 10% of reads on average were mapped to ribosomal DNA (Figure 16e). Gene expression estimates were calculated for 24,346 genes annotated in the mouse GRCm38/mm10 genome. Of these, analyses included 20,661 genes associated with a protein-coding transcript. These were further filtered to include only genes with detectable expression in mouse skin samples. Genes were considered to have detectable expression if they were associated with at least one mapped read and if the lower limit of the 95% fragments per kilobase million confidence interval was greater than zero. On the basis of these criteria, an average of 15,092 protein-coding genes had detectable expression. Cluster and principal component analysis did not identify any outliers among the four samples (Figure 16g and h).

To compare gene expression between the IMQ + IDMF and IMQ + VEH treatments, we used an exact test and negative-binomial count model, with biological variance per treatment assumed on the basis of a square root dispersion of 0.20 (R package: edgeR; R function: exactTest). Differential expression testing was performed for 15,753 protein-coding genes with detectable expression in at least one of the three samples involved in the comparison. To control the FDR, raw *P*-values were adjusted using the Benjamini–Hochberg method (Benjamini and Hochberg, 1995).

ORCIDs
Krzysztof Bojanowski: http://orcid.org/0000-0001-8692-050X
Collins U. Ibeji: http://orcid.org/0000-0003-4762-2256
Parvesh Singh: http://orcid.org/0000-0001-6742-6389
William R. Swindell: http://orcid.org/0000-0001-8504-6363
Ratan K. Chaudhuri: http://orcid.org/0000-0001-5676-9933

AUTHOR CONTRIBUTIONS
Conceptualization: KB, RKC; Data Curation: KB, WRS; Formal Analysis: KB, CUI, PS, WRS; Funding Acquisition: RKC; Investigation: KB; Methodology: CUI, PS; Project Administration: RKC; Resources: KB; Software: CUI, PS,

in c.p.m. reads. (**l**) Scatterplot. Axes represent the average expression in each group on the basis of $\log_{10}$(FPKM). In **i–l**, analyses were performed on the basis of the expression of 15,753 genes with detectable expression in at least one of the three samples involved in the differential expression comparison. In **j–l**, the number of differentially expressed genes is shown (top margin; FDR < 0.10 with FC > 1.50 or FC < 0.67). c.p.m., count per million; FC, fold change; FDR, false, discovery ratio; FPKM, fragments per kilobase million; IDMF, isosorbide di-(methyl fumarate); IMQ, imiquimod; No., number; PC, principal component; QC, quality control; VEH, vehicle.

WRS; Supervision: RKC; Validation: KB; Visualization: WRS; Writing — Original Draft Preparation: KB, WRS; Writing — Review and Editing: KB, CUI, PS, WRS, RKC.

CONFLICT OF INTEREST

Isosorbide di-(methyl fumarate) was developed and patented by Symbionyx Pharmaceuticals (Boonton, NJ). RKC is president and chief executive officer of Symbionyx Pharmaceuticals and Sytheon (Boonton, NJ) with an ownership interest in both companies. KB is a chief scientific officer of Symbionyx Pharmaceuticals and chief executive officer of Sunny BioDiscovery (Santa Paula, CA). WRS is a Symbionyx Pharmaceuticals shareholder and member of the Symbionyx Advisory Board. KB, PS, and WRS have received consulting reimbursement from Sytheon. CUI states no conflict of interest.

ACKNOWLEDGMENTS

The authors would like to thank Synthon (Boonton, NJ) for funding this research. We additionally thank Stephanie Ma (Sunny BioDiscovery, Santa Paula, CA), Geovani Quijas (Sunny BioDiscovery), Tony Chang (International Chemistry Testing, Milford, MA), and Marsha Sintara (International Chemistry Testing) for their dedicated assistance. We acknowledge the Jai Research Foundation (Vapi, India) for carrying out dermal toxicity studies, which were performed with contributions from Abhilasha Mhaske, Disha Chande, Rahul K. Vaja, Utsav N. Patel, Jaimish Prajapati, Monali Shinde, Nilesh A. Panpatil, Partha Bose, Ramesh Verma, Ritu Chhimwal, andVishvesh Dalal. Mouse imiquimod studies were performed under the supervision of Harunor Rashid (Charles River Laboratories, Montreal, Canada). We acknowledge the National Research Foundation (Pretoria, South Africa) for rated researcher funding (Grant number 126963) and the Centre for High Computing Performance in Cape Town (South Africa) for access and use of computational resources.

REFERENCES

Altmeyer PJ, Matthes U, Pawlak F, Hoffmann K, Frosch PJ, Ruppert P, et al. Antipsoriatic effect of fumaric acid derivatives. Results of a multicenter double-blind study in 100 patients. J Am Acad Dermatol 1994;30:977–81.

Anders S, Pyl PT, Huber W. HTSeq–a Python framework to work with high-throughput sequencing data. Bioinformatics 2015;31:166–9.

Ates G, Vanhaecke T, Rogiers V, Rodrigues RM. Assaying cellular viability using the neutral red uptake assay. Methods Mol Biol 2017;1601:19–26.

Atz M, Walsh D, Cartagena P, Li J, Evans S, Choudary P, et al. Methodological considerations for gene expression profiling of human brain. J Neurosci Methods 2007;163:295–309.

Bagel J, Gold LS. Combining topical psoriasis treatment to enhance systemic and phototherapy: a review of the literature. J Drugs Dermatol 2017;16:1209–22.

Becke AD. Becke's three parameter hybrid method using the LYP correlation functional. J Chem Phys 1993;98:5648–52.

Benjamini Y, Hochberg Y. Controlling the false discovery rate: a practical and powerful approach to multiple testing. J R Stat Soc Series B Stat Methodol 1995;57:289–300.

Besaratinia A, Synold TW, Chen HH, Chang C, Xi B, Riggs AD, et al. DNA lesions induced by UV A1 and B radiation in human cells: comparative analyses in the overall genome and in the p53 tumor suppressor gene. Proc Natl Acad Sci USA 2005;102:10058–63.

Boyle J, Kill IR, Parris CN. Heterogeneity of dimer excision in young and senescent human dermal fibroblasts. Aging Cell 2005;4:247–55.

Brown J, Pirrung M, McCue LA. FQC Dashboard: integrates FastQC results into a web-based, interactive, and extensible FASTQ quality control tool. Bioinformatics 2017;33:3137–9.

Brück J, Dringen R, Amasuno A, Pau-Charles I, Ghoreschi K. A review of the mechanisms of action of dimethylfumarate in the treatment of psoriasis. Exp Dermatol 2018;27:611–24.

Chaudhuri RK, Bojanowski K. WO2016160635 - compositions and methods for treating psoriasis. Symbionyx Pharmaceuticals. https://patentscope.wipo.int/search/en/detail.jsf?docId=WO2016160635; 2017. (accessed August 9, 2021).

Chiang CC, Cheng WJ, Korinek M, Lin CY, Hwang TL. Neutrophils in psoriasis. Front Immunol 2019;10:2376.

Chuang SY, Lin CH, Sung CT, Fang JY. Murine models of psoriasis and their usefulness for drug discovery. Expert Opin Drug Discov 2018;13:551–62.

DeLuca DS, Levin JZ, Sivachenko A, Fennell T, Nazaire MD, Williams C, et al. RNA-SeQC: RNA-seq metrics for quality control and process optimization. Bioinformatics 2012;28:1530–2.

Draize JH. Methods for the study of irritation and toxicity of substances applied topically to the skin and mucous membranes. J Pharmacol Exp Ther 1944;82:377–90.

Dykes IM, Emanueli C. Transcriptional and post-transcriptional gene regulation by long non-coding RNA. Genomics Proteomics Bioinformatics 2017;15:177–86.

Falcon S, Gentleman R. Using GOstats to test gene lists for GO term association. Bioinformatics 2007;23:257–8.

Frisch M, Trucks G, Schlegel H, Scuseria G, Robb M, Cheeseman J, et al. Gaussian 09, Revision D. 01, 2009, Gaussian. 2009.

Gehring W, Gloor M. Persistierende spontanerytheme durch topische anwendung von fumarsäuremonoethylester–eine obligate mastzelldegranulation? [Persistent spontaneous erythema caused by topical use of fumaric acid monoethyl ester–an obligate mast cell degranulation?]. Dermatol Monatsschr 1990;176:123–8 [in German].

Gene Ontology Consortium, Blake JA, Dolan M, Drabkin H, Hill DP, Li N, et al. Gene Ontology annotations and resources. Nucleic Acids Res 2013;41:D530–5.

Gentleman RC, Carey VJ, Bates DM, Bolstad B, Dettling M, Dudoit S, et al. Bioconductor: open software development for computational biology and bioinformatics. Genome Biol 2004;5:R80.

Gerdes S, Shakery K, Mrowietz U. Dimethylfumarate inhibits nuclear binding of nuclear factor kappaB but not of nuclear factor of activated T cells and CCAAT/enhancer binding protein beta in activated human T cells. Br J Dermatol 2007;156:838–42.

Gesser B, Johansen C, Rasmussen MK, Funding AT, Otkjaer K, Kjellerup RB, et al. Dimethylfumarate specifically inhibits the mitogen and stress-activated kinases 1 and 2 (MSK1/2): possible role for its anti-psoriatic effect. J Invest Dermatol 2007;127:2129–37.

Gesser B, Rasmussen MK, Raaby L, Rosada C, Johansen C, Kjellerup RB, et al. Dimethylfumarate inhibits MIF-induced proliferation of keratinocytes by inhibiting MSK1 and RSK1 activation and by inducing nuclear p-c-Jun (S63) and p-p53 (S15) expression. Inflamm Res 2011;60:643–53.

Gillard GO, Collette B, Anderson J, Chao J, Scannevin RH, Huss DJ, et al. DMF, but not other fumarates, inhibits NF-κB activity in vitro in an Nrf2-independent manner. J Neuroimmunol 2015;283:74–85.

Gonzalez C, Schlegel HB. An improved algorithm for reaction path following. J Chem Phys 1989;90:2154–61.

Gonzalez C, Schlegel HB. Reaction path following in mass-weighted internal coordinates. J Phys Chem 1990;94:5523–7.

Hannon GJ. FASTX-toolkit. http://hannonlab.cshl.edu/fastx_toolkit/; 2010. (accessed August 11, 2021).

Held KD, Epp ER, Awad S, Biaglow JE. Postirradiation sensitization of mammalian cells by the thiol-depleting agent dimethyl fumarate. Radiat Res 1991;127:75–80.

Helwa I, Choudhary V, Chen X, Kaddour-Djebbar I, Bollag WB. Anti-psoriatic drug monomethylfumarate increases nuclear factor erythroid 2-related factor 2 levels and induces aquaporin-3 mRNA and protein expression. J Pharmacol Exp Ther 2017;362:243–53.

Helwa I, Patel R, Karempelis P, Kaddour-Djebbar I, Choudhary V, Bollag WB. The antipsoriatic agent monomethylfumarate has antiproliferative, pro-differentiative, and anti-inflammatory effects on keratinocytes. J Pharmacol Exp Ther 2015;352:90–7.

Irizarry RA, Bolstad BM, Collin F, Cope LM, Hobbs B, Speed TP. Summaries of Affymetrix GeneChip probe level data. Nucleic Acids Res 2003;31:e15.

Kadam DP, Suryakar AN, Ankush RD, Kadam CY, Deshpande KH. Role of oxidative stress in various stages of psoriasis. Indian J Clin Biochem 2010;25:388–92.

Kanehisa M, Sato Y, Kawashima M, Furumichi M, Tanabe M. KEGG as a reference resource for gene and protein annotation. Nucleic Acids Res 2016;44:D457–62.

Kim D, Pertea G, Trapnell C, Pimentel H, Kelley R, Salzberg SL. TopHat2: accurate alignment of transcriptomes in the presence of insertions, deletions and gene fusions. Genome Biol 2013;14:R36.

Kim HJ, Lebwohl MG. Biologics and psoriasis: the beat goes on. Dermatol Clin 2019;37:29–36.

Kim WB, Jerome D, Yeung J. Diagnosis and management of psoriasis. Can Fam Physician 2017;63:278–85.

Kohn W, Becke AD, Parr RG. Density functional theory of electronic structure. J Phys Chem 1996;100:12974–80.

Kragballe K, van de Kerkhof PC, Gordon KB. Unmet needs in the treatment of psoriasis. Eur J Dermatol 2014;24:523–32.

Lahti A, Maibach HI. Contact urticaria from diethyl fumarate. Contact Dermatitis 1985;12:139–40.

Lee LP, Cole DJ, Payne MC, Skylaris CK. Natural bond orbital analysis in the ONETEP code: applications to large protein systems. J Comput Chem 2013;34:429–44.

Lee YJ, Bae JH, Kang SG, Cho SW, Chun DI, Nam SM, et al. Pro-oxidant status and Nrf2 levels in psoriasis vulgaris skin tissues and dimethyl fumarate-treated HaCaT cells. Arch Pharm Res 2017;40:1105–16.

Li Y, Ma F, Li H, Song Y, Zhang H, Jiang Z, et al. Dimethyl fumarate accelerates wound healing under diabetic condition. J Mol Endocrinol 2018;61:163–72.

Liu WM, Mei R, Di X, Ryder TB, Hubbell E, Dee S, et al. Analysis of high density expression microarrays with signed-rank call algorithms. Bioinformatics 2002;18:1593–9.

Lowes MA, Suárez-Fariñas M, Krueger JG. Immunology of psoriasis. Annu Rev Immunol 2014;32:227–55.

Ma S, Gobis K, Swindell WR, Chaudhuri R, Bojanowski R, Bojanowski K. Synthesis and activity of the salicylic acid ester of bakuchiol in psoriasis-surrogate keratinocytes and skin substitutes. Clin Exp Dermatol 2017;42:251–60.

Maron DM, Ames BN. Revised methods for the Salmonella mutagenicity test. Mutat Res 1983;113:173–215.

Martin M. Cutadapt removes adapter sequences from high-throughput sequencing reads. EMBnet J 2011;17:10–2.

McCall MN, Murakami PN, Lukk M, Huber W, Irizarry RA. Assessing Affymetrix GeneChip microarray quality. BMC Bioinformatics 2011;12:137.

Menter A, Korman NJ, Elmets CA, Feldman SR, Gelfand JM, Gordon KB, et al. Guidelines of care for the management of psoriasis and psoriatic arthritis: section 3. Guidelines of care for the management and treatment of psoriasis with topical therapies. J Am Acad Dermatol 2009;60:643–59.

Mitchell DL. The relative cytotoxicity of (6–4) photoproducts and cyclobutane dimers in mammalian cells. Photochem Photobiol 1988;48:51–7.

Mortelmans K, Zeiger E. The Ames Salmonella/microsome mutagenicity assay. Mutat Res 2000;455:29–60.

Mrowietz U, Szepietowski JC, Loewe R, van de Kerkhof P, Lamarca R, Ocker WG, et al. Efficacy and safety of LAS41008 (dimethyl fumarate) in adults with moderate-to-severe chronic plaque psoriasis: a randomized, double-blind, Fumaderm® - and placebo-controlled trial (Bridge) [published correction appears in Br J Dermatol 2018;178:308]. Br J Dermatol 2017;176:615–23.

Mukherjee S, Date A, Patravale V, Korting HC, Roeder A, Weindl G. Retinoids in the treatment of skin aging: an overview of clinical efficacy and safety. Clin Interv Aging 2006;1:327–48.

Nieboer C, de Hoop D, van Loenen AC, Langendijk PN, van Dijk E. Systemic therapy with fumaric acid derivates: new possibilities in the treatment of psoriasis. J Am Acad Dermatol 1989;20:601–8.

Pratt IS. Global harmonisation of classification and labelling of hazardous chemicals. Toxicol Lett 2002;128:5–15.

Reszke R, Szepietowski JC. A safety evaluation of dimethyl fumarate in moderate-to-severe psoriasis. Expert Opin Drug Saf 2020;19:373–80.

Salmon AB, Ljungman M, Miller RA. Cells from long-lived mutant mice exhibit enhanced repair of ultraviolet lesions. J Gerontol A Biol Sci Med Sci 2008;63:219–31.

Schäfer GN. Fumarsäure lindert die Schuppenflechte. Selecta 1984;15:1260–1 [in German].

Sebök B, Bonnekoh B, Geisel J, Mahrle G. Antiproliferative and cytotoxic profiles of antipsoriatic fumaric acid derivatives in keratinocyte cultures. Eur J Pharmacol 1994;270:79–87.

Seidel P, Merfort I, Tamm M, Roth M. Inhibition of NF-κB and AP-1 by dimethylfumarate correlates with down-regulated IL-6 secretion and proliferation in human lung fibroblasts. Swiss Med Wkly 2010;140:w13132.

Smyth GK. Linear models and empirical bayes methods for assessing differential expression in microarray experiments. Stat Appl Genet Mol Biol 2004;3. Article3.

Stoof TJ, Flier J, Sampat S, Nieboer C, Tensen CP, Boorsma DM. The antipsoriatic drug dimethylfumarate strongly suppresses chemokine production in human keratinocytes and peripheral blood mononuclear cells. Br J Dermatol 2001;144:1114–20.

Swindell WR, Bojanowski K, Chaudhuri RK. A novel fumarate, isosorbide di-(methyl fumarate) (IDMF), replicates astrocyte transcriptome responses to dimethyl fumarate (DMF) but specifically down-regulates genes linked to a reactive phenotype. Biochem Biophys Res Commun 2020;532:475–81.

Swindell WR, Johnston A, Xing X, Little A, Robichaud P, Voorhees JJ, et al. Robust shifts in S100a9 expression with aging: a novel mechanism for chronic inflammation. Sci Rep 2013;3:1215.

Swindell WR, Remmer HA, Sarkar MK, Xing X, Barnes DH, Wolterink L, et al. Proteogenomic analysis of psoriasis reveals discordant and concordant changes in mRNA and protein abundance. Genome Med 2015a;7:86.

Swindell WR, Sarkar MK, Liang Y, Xing X, Gudjonsson JE. Cross-disease transcriptomics: unique IL-17A signaling in psoriasis lesions and an autoimmune PBMC signature. J Invest Dermatol 2016;136:1820–30.

Swindell WR, Sarkar MK, Stuart PE, Voorhees JJ, Elder JT, Johnston A, et al. Psoriasis drug development and GWAS interpretation through in silico analysis of transcription factor binding sites. Clin Transl Med 2015b;4:13.

Swindell WR, Stuart PE, Sarkar MK, Voorhees JJ, Elder JT, Johnston A, et al. Cellular dissection of psoriasis for transcriptome analyses and the post-GWAS era. BMC Med Genomics 2014;7:27.

Thio HB, Zomerdijk TP, Oudshoorn C, Kempenaar J, Nibbering PH, van der Schroeff JG, et al. Fumaric acid derivatives evoke a transient increase in intracellular free calcium concentration and inhibit the proliferation of human keratinocytes. Br J Dermatol 1994;131:856–61.

Trapnell C, Roberts A, Goff L, Pertea G, Kim D, Kelley DR, et al. Differential gene and transcript expression analysis of RNA-seq experiments with TopHat and Cufflinks [published correction appears in Nat Protoc 2014;9:2513]. Nat Protoc 2012;7:562–78.

Vandermeeren M, Janssens S, Wouters H, Borghmans I, Borgers M, Beyaert R, et al. Dimethylfumarate is an inhibitor of cytokine-induced nuclear translocation of NF-kappa B1, but not RelA in normal human dermal fibroblast cells. J Invest Dermatol 2001;116:124–30.

Veilleux MS, Shear NH. Biologics in patients with skin diseases. J Allergy Clin Immunol 2017;139:1423–30.

Wang L, Wang S, Li W. RSeQC: quality control of RNA-seq experiments. Bioinformatics 2012;28:2184–5.

Zhu QG, Hu JH, Liu JY, Lu SW, Liu YX, Wang J. Stereoselective characteristics and mechanisms of epidermal carboxylesterase metabolism observed in HaCaT keratinocytes. Biol Pharm Bull 2007;30:532–6.